

NPS-57ZI73021A

# NAVAL POSTGRADUATE SCHOOL

## Monterey, California



ELECTROHYDRODYNAMICS (EHD)

RESEARCH

BY

Oscar Biblarz

12 February 1973

Approved for public release; distribution unlimited.

F 100000

L 202. 4/3; NPS 55-572 173021A

NAVAL POSTGRADUATE SCHOOL  
Monterey, California

Rear Admiral Mason Freeman  
Superintendent

M. U. Clauser  
Provost

ABSTRACT:

This report contains further considerations of the slip parameter for unsteady flow. Several important gas/particle combinations are represented and conclusions regarding electrical efficiency are given. Also, a computer study which solves the combined Laplace/Poisson equations for geometries representing the EHD channel is included. This program is used to predict the effect of voltage-scheduling electrodes, and the predictions are checked out experimentally.



## FOREWORD

This is the final year-end report under the EHD research contract. The work was sponsored by the Naval Air Systems Command under the cognizance of Dr. H. R. Rosenwasser.

One Engineer's thesis was generated during this period and it is included in the Appendix. A paper was presented at the 7th Intersociety Energy Conversion Engineering Conference held in San Diego, California. A progress paper was given also at the energy conversion program review held at China Lake, California. A paper entitled, "Charge Depletion Mechanism Operative in Space Charge Flows," coauthored with LCDR Bohley has been accepted for publication in the Journal of Applied Physics.



## TABLE OF CONTENTS

	PAGE
I. INTRODUCTION . . . . .	1
II. SLIP PARAMETER . . . . .	4
III. DISCUSSION . . . . .	7
IV. CONCLUSIONS . . . . .	9
REFERENCES . . . . .	10
APPENDIX - Computer Modeling of Space Charge Flow in an Electrostatic Generator	
DISTRIBUTION LIST . . . . .	11





## LIST OF FIGURES (MAIN TEXT)

FIGURE		PAGE
1	Frequency Response as a Function of Effective Radius	6
2	Mixing of Jets Unsteadiness	9

## LIST OF SYMBOLS (MAIN TEXT)

$E$	= field strength
$E_b$	= breakdown field strength
$m_p$	= mass of particle
$q$	= total charge of particle
$R$	= radius of particle (spherical shape equivalent)
$S$	= total slip parameter
$S(\omega)$	= spectral slip parameter
$v_D$	= particle drift velocity
$V(\omega)$	= spectral gas velocity
$U_\infty(\text{rms})$	= root-mean-square gas velocity
$\eta_E$	= electrical efficiency
$\mu$	= mobility
$\mu_\infty$	= viscosity of gas
$\xi$	= correction factor
$\rho_p$	= particle density
$\tau_v$	= particle equilibration time
$\omega$	= frequency
$\omega_1$	= maximum frequency



## I. INTRODUCTION

EHD devices should have stage efficiencies above 10% if they are to achieve a competitive standing as electrical power generators. Although the highest efficiencies are calculated for low mobility particles, a low slip parameter for steady flow may yield incorrect efficiency values if there exist significant levels of turbulence in the flow. This unsteadiness may arise from several sources, a particular one being the mixing region of two flows. Mixing of jets is designed to improve diffuser performance and hence the EHD generator efficiency.<sup>1</sup> Another important source of turbulence in a channel is the boundary layer; the generator is inherently a high surface-to-volume ratio device and it is expected that the boundary layers are fully developed. Turbulent boundary layers would then introduce significant levels of unsteadiness.

As shown in previous reports<sup>2,3</sup>, a consideration of unsteady flow has led to the definition of a more complete slip parameter. The important equations are summarized on page 2. The momentum equation used is a simplified one and more exact descriptions would seem desirable; however, Barreto<sup>4</sup> has shown that major effects are included in the above mentioned description. Certainly, many treatises are today available<sup>5,6,7</sup> which describe the drag of micron-sized particles. Boothroyd<sup>7</sup>, for example, in a recently published book summarizes some of the information. It is shown in Boothroyd's book that for Reynolds numbers below ten and for particle-to-fluid density ratios greater than 1000, the equilibration time given by Stokes law is quite accurate. Another criticism of the analysis may be that the perturbation approach is only good for small efficiencies. This is indeed true; however, there is no compromise needed for the anemometer application described in previous reports. The efficient generator would have to be described with the full complement of conservation

### PARTICLE MOMENTUM EQUATION

$$m_p \frac{d\vec{v}_p}{dt} = 6 \pi R \mu_\infty \left( \vec{v}_\infty - \vec{v}_p \right) + q \vec{E}$$

Stroke's Drag

Electric  
Force

$m_p$  = mass of particle

$R$  = radius of particle

$q$  = charge of particle

$v_p$  = velocity of particle

$\mu_\infty$  = viscosity of fluid

$v_\infty$  = velocity of fluid

### PARTICLE EQUILIBRATION TIME

$$\tau_v = \frac{m_p}{6 \pi R \mu_\infty}$$

### PARTICLE MOBILITY (VANISHING MASS)

$$\mu = \frac{q}{6 \pi R \mu_\infty}$$

### PARTICLE SLIP

$$S = \frac{v_D}{v_\infty}$$

$$\text{Steady flow: } S = \frac{\mu E}{v_\infty}$$

$$\text{Unsteady flow: } S_{\max} = \frac{\mu E_b}{V(\omega)} + \tau_v \omega$$

$\omega$  = frequency

equations. One last area of error might be the fact that modeling spherical particles is not altogether realistic since droplets may easily deform and since information on solids indicates a variety of shapes. Here, however, a correction factor may be all that is needed to remedy the situation.

Perhaps the toughest problem in EHD is the knowledge of the size and charge distribution of the charged particles. Some information as to stability of droplet size and stability of charge per particle is also needed. For example, droplets may break up or coalesce under the pressures that exist under power generation conditions. Some charge depletion may occur<sup>8</sup> in the interelectrode space. Hence, only after an injector's operating characteristics are accurately known can improvements be incorporated toward optimum conditions. A tough problem also exists in the open-cycle EHD channel if solid particles enter the atmosphere in large quantities because this represents a health hazard.

In this report further consideration is given to the slip parameter for unsteady flow. Also, a computer study and some experimentation relevant to potential distributions inside the generator are included in the Appendix. There, some preliminary work on the measurement of mobility by the Rutherford method as outlined by Darrow<sup>9</sup> can be found. The computer study was stimulated by the work of Minardi<sup>10</sup>.



## II. SLIP PARAMETER

The criterion previously stated for slip in turbulent flow is

$$\frac{\mu E_b}{V'(\omega)} + \tau_v \omega \leq 1.0 \quad (1)$$

Now for particles of density  $\rho_p$ , the mass is given by

$$m_p = \xi^2 \otimes \left( \frac{4}{3} \pi R^3 \rho_p \right) \quad (2)$$

where  $\xi^2$  is a correction factor which accounts for non-spherical shapes.

This factor can best be defined empirically.

Hence

$$\tau_v \omega = \frac{\xi^2 \frac{4\pi}{3} R^3 \rho_p}{6\pi R \mu_\infty} \omega = \frac{2}{9} \frac{\rho_p (\xi R)^2}{\mu_\infty} \omega \quad (3)$$

Let  $\tilde{R} = \xi R$  the effective particle radius

$$\tau_v \omega = \frac{2}{9} \frac{\rho_p \tilde{R}^2}{\mu_\infty} \omega \quad (4)$$

Figure 1 shows two sets of curves bracketing a region for which the contribution of  $\tau_v \omega$  to the slip is between  $10^{-3}$  and  $10^{-2}$ . Water and mercury droplets are shown because they have been considered most extensively, but solid particles may be advantageous for some applications. Polystyrene latexes are commercially available in average diameters of  $0.1 \mu\text{m}$  to  $100 \mu\text{m}$ . Returning to Figure 1, for less dense particles the curves move to the right which is a desirable effect from practical considerations since it is easier to obtain and charge larger diameter particles. The curves in Figure 1 can, of course, be generalized to any particle/gas combination by plotting  $\rho_p \omega / \mu_\infty$  vs.  $\tilde{R}$  for whatever values of slip are desired.

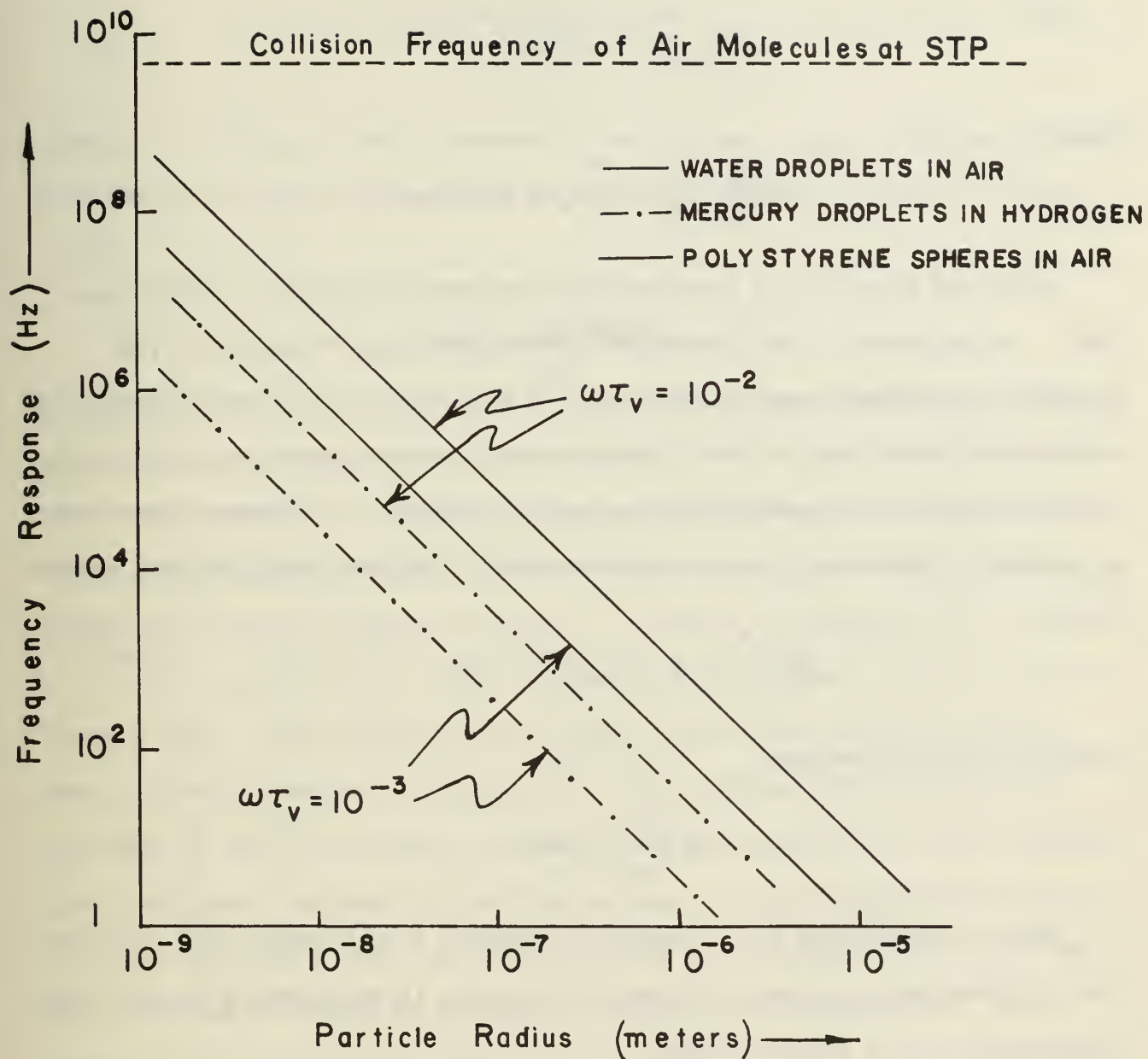


FIGURE 1. Frequency Response as a Function of Effective Radius

In order to arrive at the total slip we have to integrate  $S(\omega)$ . If we define

$$\int_0^{\infty} V(\omega) d\omega = U_{\infty}(\text{rms}) \quad (5)$$

then

$$S \leq \frac{kE}{U_{\infty}} + \frac{1}{U_{\infty}} \int_0^{\infty} \tau_V \omega V(\omega) d\omega \quad (6)$$

One would have to know experimentally the spectral density distribution,  $V(\omega)$ . As reported in the literature<sup>11</sup>, with increasing frequencies  $V(\omega)$  is found to be proportional first to  $\omega^{-5/3}$  and later to  $\omega^{-7}$ , which corresponds to a rather abrupt drop at the high frequencies. For illustrative purposes, a simplification will be made here by assuming that  $V(\omega)$  is a constant value until  $\omega_1$  and zero thereafter (i.e., a step function). The resulting integral becomes

$$\frac{1}{U_{\infty}} \int_0^{\infty} \tau_V \omega V(\omega) d\omega = \tau_V \omega_1 \quad (7)$$

and hence the slip becomes

$$S \leq \frac{kE}{U_{\infty}} + \tau_V \omega_1 \quad (8)$$

This is reminiscent of our earlier statements to the effect that consideration of the highest frequency for which  $V(\omega)$  has a large intensity is all that is necessary in the simplest cases.

We can now define the electrical efficiency or internal efficiency of energy conversion<sup>12</sup>

$$\eta_E \approx \frac{1}{1 + \frac{\mu E \cdot E}{V \cdot E}} = \frac{1}{1 + S} \quad (9)$$



Upon substitution of Equation 8, the above becomes

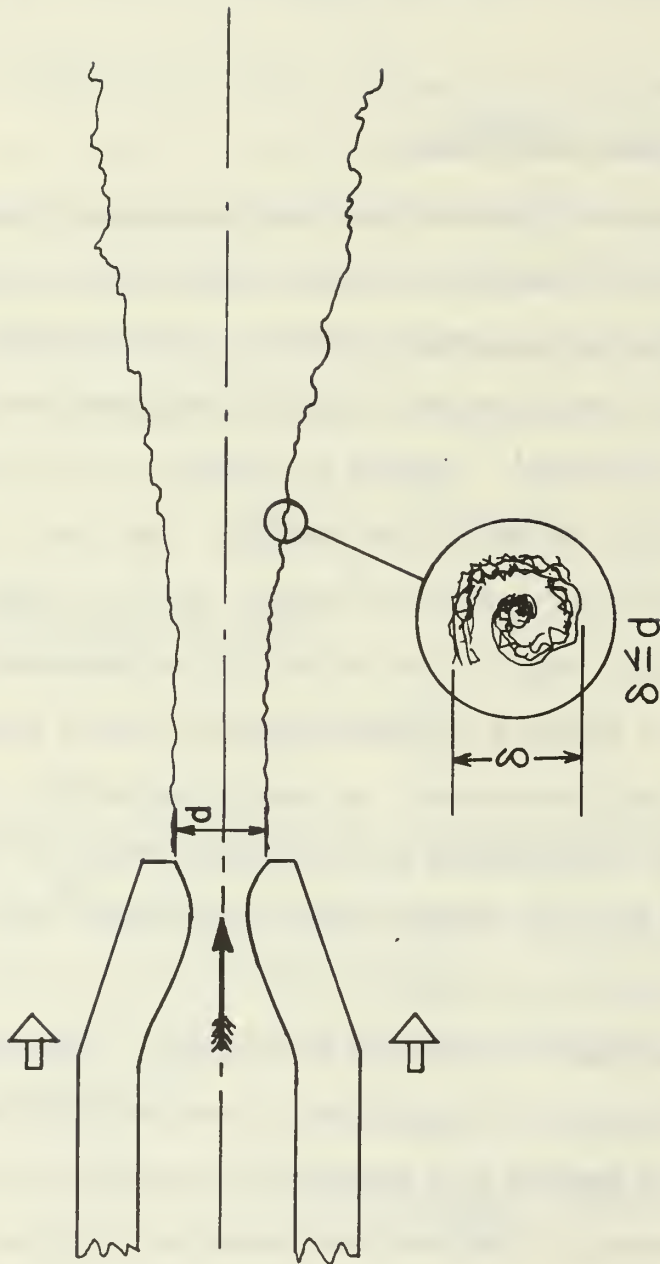
$$\eta_E \approx \frac{1}{1 + \left( \frac{kE}{U_\infty} + \tau_v \omega_1 \right)} \quad (10)$$

Clearly, if  $kE/U_\infty$  is small compared to one but not  $\tau_v \omega_1$ , then the efficiency will be low, perhaps falling below the 10% value alluded to earlier in this report.

### III. DISCUSSION

While it is difficult to talk in generalities, some appropriate comments can be made here about the mixing of two jets. When a supersonic jet carrying the charged particles is injected into a subsonic flow of a low molecular weight gas, a highly efficient diffuser results which improves generator performance by the high pressure operation<sup>1</sup>. Suppose we consider a jet of mercury at 300 m/sec issuing from a nozzle one mm in exit diameter. The size of the largest eddies, which initially carry most of the energy, can be no larger than the nozzle diameter. In fact, most of the eddies will be generated at the edges of the jet as shown in Figure 2, so that taking the nozzle diameter gives the lowest frequency to the fluctuations. An eddy characteristic time is of the order of  $3 \times 10^{-6}$  sec corresponding to a frequency of  $3 \times 10^5$  sec<sup>-1</sup>. Now, returning to Figure 1, we must have droplet radii of about  $10^{-8}$  m to realize a low total slip for this kind of flow.

This diameter is quite small and droplets may be unstable. Calculations of the drag for this type of particle are complicated by the fact that the particles do not interact in the fashion of a continuum if conditions are near STP. Moreover, the thermal control of the generator system may be quite complex in order to get  $10^{-8}$  m particles from a condensing system (powders, on the other hand, would be nearly impossible to handle).



FOR  $a = 3 \times 10^2 \text{ M/Sec}$ ,  $d = 1 \text{ mm}$

$T_{\max} \approx \frac{d}{a} = 3 \times 10^{-6} \text{ Sec}$       Eddy Char. Time

$\omega \approx 3 \times 10^5 \text{ Sec}^{-1}$       Droplet Radius  $\approx 10^{-8} \text{ M}$

FIGURE 2. Mixing of Jets Unsteadiness

What can we surmise will happen if the particles are substantially greater than the low slip value of  $10^{-8}$  m? First of all, the diffuser effect will still take place but the particles will not be intimately coupled to the flow. Particle inertia will influence their trajectories. This could have a strong effect on the growth of the particles in the mixing region as well as on the mixing itself. Mixing of charges, it will be recalled, is one of the things that affects breakdown. Jet profiles may differ when the jet contains a large number of high slip particles and the positioning of electrodes and of voltage-scheduling surface is thereby complicated. In short, performance estimates based on a steady flow slip parameter will differ from actuality and they will differ by underestimating losses.

#### IV. CONCLUSIONS

In this report, an analysis has been presented which permits the calculation of efficiency when experimental information for the velocity spectral distribution is available. The effects of turbulence may vary from larger slip and frictional losses to an enhancement of the breakdown potential. The field of diagnostics in space-charge flows remains underdeveloped and thus our models suffer from the lack of validating experimental information (current-voltage data from the generator represents the composite action of many processes and is not useful in this regard).

## References

1. M. Lawson and H. von Ohain, "Electrofluid Dynamic Energy Conversion Present Status and Research Areas," Journ. of Energy for Industry, Paper No. 70-Ener-A, ASME 1971.
2. O. Biblarz, "Electrohydrodynamics (EHD) Research," NPS-57Zi71121A, 10 December 1971.
3. O. Biblarz, K. E. Woehler, and T. H. Gawain, "EHD Research," NPS-57ZI0121A, 30 Dec. 1970.
4. E. Barreto, "Research on Power Generation Electrogasdynamic Energy Converter," ARL 67-0008 January 1967.
5. N. A. Fuchs, Mechanics of Aerosols, Elmsford, New York, 1964.
6. S. L. Soo, Fluid Dynamics of Multiphase Systems, Blaskell Pub. Co., Waltham, Mass.
7. R. G. Boothroyd, Flowing Gas-Solids Suspension, Chapman and Hall, London 1971
8. O. Biblarz and C. M. Bohley "Charge Depletion Mechanism Operative in Space Charge Flow," accepted for publication in JAP.
9. K. K. Darrow, Electrical Phenomena in Gases, Williams and Wilkins Co., London 1932.
10. J. E. Minardi, "Computer Program for the Calculation of Electric Fields in an Electrofluidynamic Generator," ARL 68-0156 August 1968.
11. H. Schlichting, Boundary-Layer Theory, McGraw-Hill, NY 1968.
12. O. M. Stuetzer, "Magnetohydrodynamics and Electrohydrodynamics," Physics of Fluids, 3, 534, May 1962.

APPENDIX

# NAVAL POSTGRADUATE SCHOOL

## Monterey, California



# THESIS

Computer Modeling of Space Charge Flow  
in an Electrogasdynamic Generator

by

Carl Martin Bohley

Thesis Advisor:

O. Biblarz

June 1972

*Approved for public release; distribution unlimited.*



## ABSTRACT

In an electrogasdynamic (EGD) generator the flow of a neutral medium carrying unipolar electrical charges constitutes an electrical current. A model of the charge flow in an EGD generator was constructed for use in a computer program. The program is designed to solve Poisson's and Laplace's equations for both axisymmetric and two-dimensional geometries. Schlieren photographs of the charge cloud were used to determine the charge cloud profile required by the program. Computer generated predictions agreed with three known solutions to Poisson's equation. Computer predictions of the effects of space charge flow modification were obtained. Space charge flow was modified both by increasing flow speed and by manipulating the space charge electric field. Experimentally, this was accomplished by increasing flow stagnation pressure and by application of a separate controllable electric field. Experimental results compare favorably with computer predictions. Some measurements were also made of the mobility range of the charged particles.

## TABLE OF CONTENTS

I.	INTRODUCTION -----	8
II.	THEORETICAL CONSIDERATIONS -----	10
III.	PROGRAMMING CONSIDERATIONS -----	16
IV.	DESCRIPTION OF APPARATUS -----	21
V.	EXPERIMENTAL PROCEDURE -----	23
VI.	RESULTS AND DISCUSSION -----	25
VII.	CONCLUSIONS -----	29
VIII.	RECOMMENDATIONS -----	30
	APPENDIX A: NORMALIZATION PROCEDURE -----	31
	APPENDIX B: FINITE DIFFERENCE EQUATION DERIVATION -----	33
	APPENDIX C: PROGRAM DESCRIPTION -----	36
	APPENDIX D: MOBILITY MEASUREMENTS -----	44
	FIGURES -----	46
	COMPUTER PROGRAM -----	65
	BIBLIOGRAPHY -----	83
	INITIAL DISTRIBUTION LIST -----	84
	FORM DD 1473 -----	85

## LIST OF ILLUSTRATIONS

1.	EGD Generator Schematic -----	46
2.	Sample EGD Geometry and Boundary Conditions -----	47
3.	Parallel Electrode Potential Distribution at Breakdown --	48
4.	Aerosol Injector and Collector Probe -----	49
5.	Steam Jet Schlieren Photographs -----	50
6.	Steam Jet Profile -----	51
7.	Guard Ring Schematic -----	52
8.	Corona Current and Convection Current Ratio vs. Corona Voltage -----	53
9.	Potential Distribution, $P_o = 8$ psig, $\rho_{eo} = .0103 \text{ C/m}^3$ ---	54
10.	Potential Distribution, $P_o = 14$ psig, $\rho_{eo} = .0084 \text{ C/m}^3$ --	55
11.	Centerline Distribution of Slip Parameter -----	56
12.	Potential Distribution, $\rho_{eo} = 0.0 \text{ C/m}^3$ (LAPLACIAN) -----	57
13.	Electric Field Distribution, $P_o = 14$ psig, $\rho_{eo} = .0084 \text{ C/m}^3$ -----	58
14.	Collector Current Increase Due to Guard Ring -----	59
15.	Potential Distribution, $P_o = 14$ psig, Guard Ring Voltage = 0 -----	60
16.	Potential Distribution, $P_o = 14$ psig, Guard Ring Voltage = 1kV -----	61
17.	Potential Distribution, $P_o = 14$ psig, Guard Ring Voltage = 2kV -----	62
18.	Comparison Between Laplacian $\vec{E}$ field Distribution and Poisson $\vec{E}$ Field Distribution Using the Guard Ring -----	63
19.	Mobility Measuring Schematic -----	64



## TABLE OF SYMBOLS AND ABBREVIATIONS

A	Normalized potential; Argon; ampere
$A_{i,j}$	Normalized potential at grid point (i,j)
$\bar{B}$	Magnetic flux density (Wb/m <sup>2</sup> )
C	Constant resulting from normalization; Coulomb
$\bar{E}$	Electric field intensity (V/m)
EGD	Electrogasdynamics
$\bar{E}_{app}$	Electric field due to voltage applied to physical geometry (V/m)
$\bar{E}_b$	Breakdown field strength (V/m)
$\bar{E}_{sc}$	Electric field due to space charge presence (V/m)
$\tilde{E}$	Normalized $\bar{E}$ field from computer solution
F	Fahrenheit
HL	Mesh interval
$h_o$	Streamline stagnation enthalpy
$I_G$	Collector current (microamperes)
$I_T$	Corona current (microamperes)
$\bar{J}$	Current density (A/m <sup>2</sup> )
k	Mobility (m <sup>2</sup> /V-s)
kV	Kilovolts
M	Mach number
m	Meters
mm	Millimeters
N <sub>2</sub>	Nitrogen
P	Ambient Pressure (psig)
P <sub>o</sub>	Stagnation pressure (psig)
psig	Pounds per square inch gauge

psia	Pounds per square inch absolute
R	Normalized jet radius
r	Dielectric gas jet radius (centimeters)
$r_0$	Injector nozzle radius (centimeters)
S	Streamline entropy
SOR	Successive over-relaxation
V	Volts
$\bar{v}_p$	Total particle velocity (m/s)
$\bar{v}_\infty$	Dielectric flow velocity (m/s)
Z	Normalized axisymmetric axial coordinate
$\gamma$	Ratio of specific heats
$\delta$	Slip parameter
$\epsilon_0$	Dielectric constant for vacuum and gas (V-m/A-s)
$\rho$	Normalized space charge density
$\rho_e$	Space Charge density (C/m <sup>3</sup> )
$\rho_{eo}$	Space charge density at injector nozzle exit plane (C/m <sup>3</sup> )
$\sigma$	Maximum error in approximation to jet profile
$\phi$	Potential function
$\omega$	Over-relaxation factor , vorticity

## I. INTRODUCTION

Electrostatic phenomena involve many everyday experiences, such as walking on a thick rug and then touching a grounded object. Practical applications of electrostatic devices range from Xerography to pollution control devices or to the van der Graaf generator [1]. Recently, interest in electrical power generation has brought attention to the electrogas-dynamic (EGD) generator. This direct energy conversion device is analogous to the van der Graaf generator and operates by convecting charges with a gas against an electric field to a point of collection. The charge flow constitutes an electrical current. The charge movement is accomplished by an exchange of momentum between the flowing dielectric medium and the charges.

The common denominator of electrostatic devices is the existence of free charges in a neutral medium or dielectric -- for the present purposes a fluid. The flow of a medium with unipolar charges is termed space charge flow and the understanding of this flow is critical to the design of the EGD generator. This thesis consists of a computer model of the space charge flow to be used as an EGD generator design tool.

The computer model has some limitations inherent to the programming itself and these are discussed in Section III. In addition, parameters such as charge mobility and velocity as well as the inputs of geometry and jet configuration are needed. These are obtained with an experimental set-up discussed in Section IV. The program is used to predict regions of breakdown, given an electrode geometry and a space charge cloud. In addition, the program is used to predict the effect of guard electrodes. These electrodes are placed for the purpose of 'smoothing' the electric

field in the conversion region, and both computer predictions and experimental results are given in Section VI for the effect of the guard ring.

## II. THEORETICAL CONSIDERATIONS

The EGD process requires producing, transporting and collecting the charges which comprise the electrical current. One means by which charges may be produced is by a corona discharge. Basically this scheme consists of two electrodes, which may be a needle and a concentric ring; the concentric ring or attractor electrode, when charged to a high positive electrical potential with respect to the grounded needle, induces the corona discharge. The corona breaks down a neutral gas initially into its electrical components: molecular ions and free electrons. The corona needle will attract the positive ions, while negative charges will tend to migrate to the attractor ring. The EGD objective, instead, is to transport a current of negative charges away from this attractor ring.

An ion's susceptibility to movement in an electric field is termed it's 'mobility', ( $k$ ). Thus the drift velocity of the ion in the corona field is determined by the product of the ion mobility and the electric field strength to which the ion is exposed. Since the mobilities of molecular ions and free electrons are high, they would migrate rapidly to the corona electrodes and be lost to EGD power generation. However, when a supersaturated vapor is present, negatively charged droplet (micron) sized particles are nucleated which, for a given charge, will have much lower mobility than an ion [2,5]. Hence, the charged particle is more suited to EGD applications [6]. To move the charged particle against an electric field, the particle must be well coupled to the dielectric flow. When the dielectric gas transports the charge to a downstream collector, against an electric field ( $\bar{E}$ ), the total charge velocity ( $\bar{v}_p$ ) may be described as the sum of the dielectric velocity



( $\bar{v}_\infty$ ) and the drift velocity ( $k\bar{E}$ ).

$$\bar{v}_p = \bar{v}_\infty + k\bar{E} \quad (1)$$

In order to obtain the highest degree of coupling, the drift velocity of the charged particle must be low compared to the dielectric velocity [4]. The charged particles are carried out of the charge production section against an electric field in the conversion section, to the charge collector. This collector consists of an equipotential metallic surface. A path through a load to ground is provided to complete the circuit started at the grounded corona electrode. See Figure (1) for a schematic of the EGD generator.

There are several limitations that pertain to the conversion process. For an EGD generator to operate as intended, the neutral gas must remain non-conducting. This implies that the electric fields to which the dielectric is subjected must remain below the dielectric strength, or breakdown field strength, ( $E_b$ ), of the gas. Fields above the dielectric strength will produce regions of high conductivity through ionization [3]. The dielectric gas or fluid is subjected to the field resulting from the applied potential through which the charged particles are carried and to internal fields generated by the presence of the charged particles. Breakdown from external fields occurs as a result of the electrode geometry. For a given voltage, the existence of a small radius of curvature will produce a large electric field. The field will exceed the dielectric strength when the radius of curvature is small enough. The range of allowable operating voltages is thus a function of the electrode spacing. In turn, the spacing of the electrodes is also a function of the fluid dynamics of the dielectric, of possible charge depletion mechanisms, of the operating pressures, and of generator size requirements.

Total charge per particle is limited by the balance between the particle surface tension and charge repulsion forces, and is known as the Rayleigh limit. In practice, however, the total charge per particle is governed by the charge production method. For particles charged in a corona field, and which grow to micron size, the number of charges is approximately two orders of magnitude less than that predicted by the Rayleigh limit [6]. These limits must be considered in the modeling of the space charge flow in an EGD device.

In general, the equations needed to describe the EGD flow will include the momentum, continuity and energy equations. These would be necessary to determine the dielectric jet profile and hence the space charge density distribution. However, if the profile can be determined experimentally, and if the energy drained from the flow is low, the required equations are reduced to three:

#### Faraday's Law

$$\nabla \times \vec{E} = \frac{\partial \vec{B}}{\partial t} \quad \begin{array}{l} \vec{E} = \text{electric field (V/m)} \\ \vec{B} = \text{magnetic flux density vector (Wb/m}^2\text{)} \end{array}$$

#### Gauss' Law

$$\nabla \cdot \vec{E} = \frac{\rho_e}{\epsilon_0} \quad \begin{array}{l} \rho_e = \text{space charge density (C/m}^3\text{)} \\ \epsilon_0 = \text{dielectric constant for vacuum and gas (V-m/A-s)} \end{array}$$

#### Charge Conservation

$$\nabla \cdot \rho_e \vec{v}_p = 0 \quad (2)$$

where the total velocity of the charged particle is given by:

$$\vec{v}_p = \vec{v}_\infty + k(\vec{E}_{app} + \vec{E}_{sc}) \quad (3)$$

and is a function of the dielectric flow speed, particle mobility, applied electric field ( $\vec{E}_{app}$ ), and the space-charge-produced electric field ( $\vec{E}_{sc}$ ).

For the EGD generator,  $\bar{B} = 0$ , and Faraday's Law takes the form,  $\nabla \times \bar{E} = 0$ . This allows  $\bar{E}$  to be defined as the negative gradient of some potential function  $\phi$ , so that  $\bar{E} = -\nabla\phi$ . Substituting into Gauss' Law, the resulting equation is known as Poisson's equation,

$$\nabla^2 \phi = -\frac{\rho_e}{\epsilon_0} \quad (4)$$

This equation is valid in the two regions of interest within the EGD channel. One, the neutral gas jet, contains the charged particles, while the second, outside the gas jet, contains no space charged. In the space-charge-free region,  $\rho_e = 0$ , and Eq. (4) reduces to the more familiar Laplace equation. Figure (1) depicts the two regions.

Although the kinetic energy of the injected gas jet is generally augmented by the transfer of momentum from a primary flow, this method of flow augmentation is not to be used here because of the resulting unsteady motion of the jet [7]. Rather, the injected flow is augmented as described in Section IV.

Reference [8] states that the jet profile may be determined by considering the equation of conservation of charges. The radius of the gas jet ( $r$ ) may be described as a function of the initial radius ( $r_0$ ), initial charge density ( $\rho_{eo}$ ), the applied electric field and the axial coordinate ( $z$ ).

$$r = r_0 \sqrt{1 + \frac{k\rho_{eo}}{(\bar{v}_\infty + k\bar{E}_{app})^2} z} \quad (5)$$

This is based on the assumption that the charge density is a function only of axial distance from the point of injection and that the particle velocity due to coupling with the neutral gas and applied field is much



greater than that due to the space charge field, i.e.,

$$\bar{v}_{\infty} + k \bar{E}_{app} \gg k \bar{E}_{sc} \quad (6)$$

Neglecting space charge effects disallows any radial velocity. Yet there must be some component of velocity. For flow along a streamline, Crocco's theorem for a steady state, which relates enthalpy ( $h_0$ ) and entropy ( $S$ ) gradients to vorticity, is given by:

$$\bar{v}_{\infty} \times \nabla \times \bar{v}_{\infty} = \nabla h_0 - T \nabla S$$

where  $\nabla \times \bar{v}_{\infty} = \omega$  is the vorticity. For the streamline defining the boundary of the gas jet, such gradients will be very large, giving rise to vorticity. The radial velocity component introduced will give a larger jet profile than that predicted by Eq. (5), leading to a reduced charge density at any given axial distance.

In general, Equations (2) and (4) are coupled through the  $\rho_e$  term, and must be solved simultaneously. Expanding the charge conservation equation:

$$\frac{\rho_e}{r} \frac{\partial}{\partial r} \bar{v}_p + \frac{\bar{v}_p}{r} \frac{\partial}{\partial r} \rho_e + \rho_e \frac{\partial}{\partial z} \bar{v}_p + \bar{v}_p \frac{\partial}{\partial z} \rho_e = 0$$

For particles of low mobility, and fields below breakdown,  $\bar{v}_{\infty}$  will predominate, and Eq. (6) will hold. If the jet is assumed to be flowing normal to two plane parallel electrodes:

$$\frac{\partial}{\partial r} \bar{v}_p = \frac{\partial}{\partial r} \bar{v}_{\infty} + k \frac{\partial}{\partial r} \bar{E}_{app} = 0$$

Then an assumption of an initial homogeneous distribution of charge at the jet entry plane will remain true at any position downstream. Thus,

$$\frac{\partial}{\partial r} \rho_e = 0$$

and the charge conservation equation becomes:

$$\nabla \cdot (\rho_e \bar{v}_p) = \rho_e \frac{\partial}{\partial z} \bar{v}_p + \bar{v}_p \frac{\partial}{\partial z} \rho_e = 0$$

This allows the cloud shape and hence the charge density to be determined solely by the fluid dynamics of the dielectric jet, and uncouples the charge conservation equation from Poisson's equation. Another approach to this problem is to determine the jet profile experimentally. An approximate analytical description is obtained by fitting a parabola to this profile. This approach is convenient in this work and the approximation becomes an integral part of the computer program.

We can now discuss the assumption of Eq. (6) that the charged particles are affected only by the gas jet and the applied field. When charged particles are injected into the conversion region, they will face the field produced by the charged particles already in the conversion section. Eventually, these charged particles will face fields which may repel all charges but those with the highest degree of viscous coupling to the gas flow. In this manner, space charge effects provide a velocity "filter" through which the gas jet must move [9].

The expression for current density ( $\bar{J}$ ) in the dielectric jet is given by:

$$\bar{J} = \rho_e \bar{v}_p$$

This expression would require a greater charge density as space charge effects slow down the charged particles in order to maintain a given current density. But as mentioned previously on Page 11, breakdown of the dielectric will occur if the space charge electric field strength is greater than the dielectric breakdown strength. This tradeoff limits the performance of the EGD generator.

### III. PROGRAMMING CONSIDERATIONS

The computer program was written for the numerical solution of Eq. (4), since closed form solutions to Poisson's equation are difficult to obtain, except in very simple cases. The program is capable of solving Poisson's equation for either an axisymmetric or two-dimensional geometry.

To facilitate the solution, Poisson's equation was normalized as described in Appendix A. In the axisymmetric form, the equation to be solved becomes:

$$\frac{1}{R} A_R + A_{RR} + A_{ZZ} = - C\rho \quad (7)$$

where A is the normalized potential and R is the normalized radius. The term on the right side is a result of the normalization described in Appendix A. In the two-dimensional equation, there is a change of variables and the radius term drops out to give the form:

$$A_{XX} + A_{YY} = - C\rho$$

By covering the geometry to be studied with a uniform square mesh, the problem may be defined in terms of a finite number of discrete points, at each of which the solution to Eq. (7) is desired. The boundaries of the mesh are determined either by the presence of electrodes at a constant potential, or by a zero normal derivative of the potential  $\phi$ . The zero normal derivative is found on an axis of symmetry, on a boundary with no normal current flow, such as an insulator, or on a boundary between two electrodes in the absence of space charge and end effects. End effects result in a distortion of the distributions about the end of a pseudo-infinite plate because of the radius of curvature of the end. Figure (2) depicts a sample geometry with appropriate boundary conditions.

The derivation of the finite difference equations for the two forms of Poisson's equation is given in Appendix B. After solving for the potential at a particular point, the form of the equation is:

$$A_{i,j} = \frac{1}{4} \left[ HL^2 C_p + A_{i+1,j} + A_{i-1,j} + A_{i,j+1} + A_{i,j-1} + \frac{HL}{2R} (A_{i,j+1} - A_{i,j-1}) \right]$$

where the subscripts represent mesh row and column, respectively. For points governed by a boundary condition of a zero normal derivative, as on an axis of symmetry, the general equation becomes:

$$A_{i,j} = 1.333 A_{i,j+1} - .333 A_{i,j+2}$$

The derivation of this equation is also given in Appendix B.

The solution method chosen is an iterative process known as "successive over-relaxation" (SOR), or the "extrapolated Liebmann method [10]." Over-relaxation introduces a factor ( $\omega$ ), by which the solution at the point in question, as a result of the previous iteration, is taken into account. By assigning the proper value to this factor, convergence rate of the solution may be maximized; however,  $\omega$  is limited by the following:

$$1 \leq \omega \leq 2$$

The method of selecting a value for  $\omega$  may be found in textbooks covering iterative solution methods such as Reference [10]. For this thesis  $\omega$  is a constant equal to 1.5. The form of the resulting equation then becomes:

$$A_{i,j}^{n+1} = A_{i,j}^n + \frac{\omega}{4} \left[ HL^2 C_p + A_{i+1,j}^n + A_{i-1,j}^{n+1} + A_{i,j-1}^n + A_{i,j+1}^{n+1} + \frac{HL}{2R} (A_{i,j+1}^n - A_{i,j-1}^{n+1}) - 4 A_{i,j}^n \right]$$



This shows that the solution at a point, on the (n+1)st iteration is dependent on the solutions at surrounding points obtained on either the (n)th or (n+1)st iteration. Convergence is determined by comparing a specified value, DELU, to the maximum potential change per iteration. The value of DELU is a data item required by the computer program and remains constant until changed by the user.

This simplification of the governing equations introduced in Section II allows the space charge density to be described as a function of the initial space charge, of jet radius and of the initial jet radius. The expression, as shown by Minardi, is:

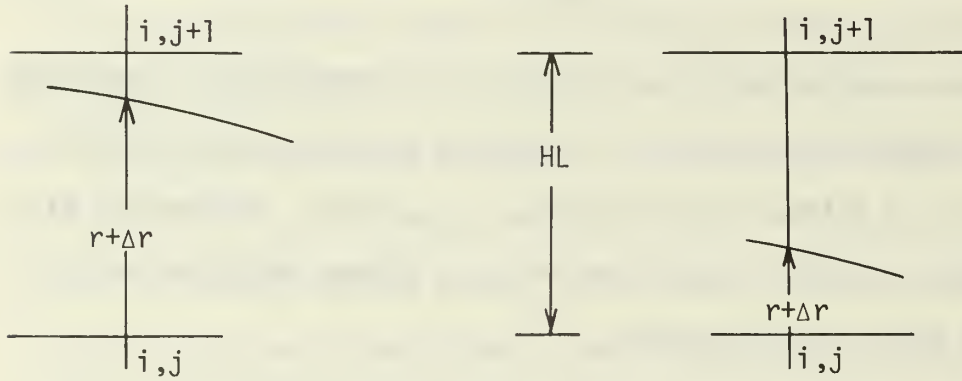
$$\rho_e = \rho_{eo} \left( \frac{r_o}{r} \right)^2 \quad (8)$$

This leads to a charge density varying with the longitudinal coordinate only and a constant distribution in the plane normal to the dielectric flow. The use of a known nozzle radius, i.e., initial jet radius, of a gas flow speed, and of a corona current ( $I_T$ ), allows determination of the injected space charge density.

Also to be considered when modeling the charge distribution is the collection process. Charged particles cannot continue to be collected indefinitely. Eventually, at some point downstream from the initial point of collection, all but a negligible part of the charged particles that are to be collected, will have been collected. Further charge contributions to the collector current will have a negligible effect on the potential distribution. It is necessary to determine where this takes place, as the boundary conditions on the problem include a zero charge density. Hence, the space charge contained in the dielectric jet is not to be carried up to the boundary of the region of interest. Using various collection lengths in the computer program, it was found

that allowing space charge to exist over 80% of the collector length gave results which changed little, less than 3%, as this collection length was increased.

In general, the jet profile does not coincide with a mesh point at any given axial coordinate. However, the program is not capable of handling a variable mesh size. In order to differentiate clearly between the regions of space charge and no space charge, the program approximates the gas jet with a series of steps in order to meet the constant mesh interval limitation. This is explained with the help of the figure below:



If  $\Delta r \geq \frac{HL}{2}$ , the gas jet is considered to be passing through the point  $(i,j+1)$ , and if  $\Delta r < \frac{HL}{2}$ , through the point  $(i,j)$ . The charge density is computed according to Eq. (8), giving a value of charge density which is then assigned to each mesh point out to, and including, the point on the approximated jet boundary. This introduces some error into the calculation process. The approximation scheme limits the displacement of the dielectric jet boundary to a maximum of  $HL/2$ . Then the maximum error ( $\sigma_{\max}$ ) is given by:

$$\sigma_{\max} = HL/2R$$

This would imply that the maximum error would occur at the minimum jet radius, the injector nozzle. By selecting the appropriate mesh interval, the radius at the nozzle can be made to coincide with a mesh point. The minimum radius at which the maximum displacement will occur is then downstream from the nozzle.  $\sigma_{\max} = 5\%$  is typical of the various mesh sizes used.

The validity and accuracy of the program was determined by comparison with the known solution for several problems. A geometry consisting of finite parallel plane electrodes, approximating infinite parallel plane electrodes, with a gap spacing of 2 cm and a potential difference of 15 kV was used to determine if the program would predict the existence of electrical breakdown across the gap as specified in [11]. Because of the method of normalization used, as described in Appendix A, the result of entering this configuration into the program is a potential distribution which varies linearly from zero to one, and a field strength of one throughout the gap, indicating that breakdown of the air gap is predicted. To attain this solution, it was found that electrode end effects had to be minimized, or a very distorted distribution would result. A pseudo-infinite plane electrode minimum length to air gap ratio of one was required to minimize the distortion. Figure (3) depicts the correct potential distribution calculated by the program once the parallelplane electrodes were properly modeled.

Results of the program were also compared with two results previously published by Minardi [2,8], concerning space charge flow between parallel infinite plane electrodes; values of the input data used were the same. A comparison of the graphical output appeared to be equivalent for the two geometries compared.

#### IV. DESCRIPTION OF APPARATUS

The need to input certain parameters to the program dictated the type and extent of the experimental work to be accomplished. This work also had to be relevant to the EGD facility that was under operation at NPS [4,5]. The program requires both the electrode geometry of interest and the dielectric gas jet profile, as inputs, so that charge density distribution may be calculated. The gas jet profile is also the means of modeling the change in a variable such as the dielectric flow speed. The effect of an increase in  $\bar{v}_{\infty}$  was of particular interest because a larger  $\bar{v}_{\infty}$  would increase the dominance of the first term on the right of Eq. (1). Also of interest was the effect of the guard ring electrode on the space charge flow. These two experiments, increasing  $\bar{v}_{\infty}$  and the use of the guard ring, were also required for correlation of the trends in experimental results with those trends predicted by the computer program.

The EGD channel to be modeled consists of a charged aerosol injector and a collector probe. See Figure (4) for dimensions. The vapor for the aerosol is generated by a modified Hotshot model MB-31 electric steam boiler, pressure fed with distilled water. To obtain best results, it was found necessary to ensure that the entire steam generating system was free of any impurities. The corona needle is grounded through a Simpson microammeter, while the attractor ring is powered by a Sorenson high voltage supply, with a range of zero to ten kV. The power supply output is monitored by a Sensitive Research high impedance voltmeter connected across the corona attractor ring gap. The collector needle is grounded through a Simpson microammeter in series with a diode to prevent reverse current flow [7].



In order to determine the jet profile, Schlieren photographs of the steam jet were taken. The setup consists of mirrors, a collimated light source, a knife-edge and a camera. Photographs of the jet were taken with stagnation pressures of 8, 10 and 14 psig. A horizontal knife-edge was used to more clearly define the vertical gradient across the jet boundary. The Schlieren photographs of the 8 and 14 psig jet are shown in Figure (5). The photographs show a high pressure jet (14 psig) approximately 100% larger than the given by Eq. (5). The resulting jet profiles are shown in Figure (6).

In order to determine the effects of manipulating the electric field distribution, a field entirely separate from that of the corona was applied by means of a 'guard electrode', in the form of a ring of stainless steel. Internal diameters used ranged from  $\frac{3}{8}$  of an inch to  $\frac{3}{16}$  of an inch. The ring was mounted on a plexiglass insulator, supported by a stainless steel rod. The rod was mounted on a vernier allowing the position of the ring to be varied along the longitudinal axis of the collector needle. The voltage applied to the guard ring was supplied by a Spellman high voltage power supply. The output voltage of the power supply was determined by calibration of the power supply voltmeter with the Sensitive Research voltmeter. This was necessary because the Spellman voltmeter does not indicate line voltage. The guard ring schematic is shown in Figure (7).

## V. EXPERIMENTAL PROCEDURE

Initial experiments with the guard ring were carried out at eight psig. The temperatures used corresponded to vapor states at either side of saturated vapor, similar to previous EGD work [4,5,7]. At this low pressure, a severe deterioration of the 'convection current' ratio, (collector current/corona current), was encountered as ring voltage was increased. This appeared to be the result of too low a dielectric velocity and hence a high slip parameter (i.e., a high ratio of the drift velocity to the dielectric velocity). The charged particles were diverted from the collector, being attracted to the guard ring. For this reason and for the desire to improve the generator performance without the ring, it was decided to increase the flow rate of the dielectric by increasing the reservoir pressure. Stagnation conditions were changed by the introduction of a separate 'dry' gas into the steam boiler.

The baseline characteristics of the EGD channel were determined by supplying steam to the corona discharge at eight psig and 240-245°F. Corona voltage was varied over a range of zero to three kV, and values of corona current and collector current were recorded. The collector probe was positioned 5 mm downstream from the nozzle exit plane. Dry gases used were both  $N_2$  and A. The choice of gas appeared to make no difference in the results. Introducing the dry gases was done by regulating the flow of gas from a standard high pressure gas bottle. The gas was introduced into the boiler through a check valve operating at 10 psig. With the boiler operating at 8 psig, the high pressure gas was used to raise the operating pressure of the boiler to approximately

13.5 psig. After allowing the rate of steam production to stabilize, resultant stagnation pressure was 14 psig.

To determine the effects of the 'guard electrode', a baseline performance with no guard ring was run at 14 psig. Once this was established, the trailing edge of the guard ring was placed in one of three positions, either 2 mm upstream, coincident with, or 2 mm downstream of the collector needle tip. At each guard ring position, the applied potential was varied over a range of 0 - 3.5 kV, and effects on collector current were recorded. Rings of various sizes were used. When rings smaller than  $\frac{3}{8}$  of an inch diameter were used, breakdown occurred, apparently caused by stray droplets providing a direct path for current transmission. Condensation of the steam inside the ring was also observed, and was a possible factor contributing to breakdown.

## VI. RESULTS AND DISCUSSION

The introduction of a high pressure gas into the system resulted in collected currents of two to three times greater than the low pressure steam. Figure (8) shows the baseline (8 psig) corona current-voltage curve and the corona current-voltage curve for the high pressure steam jet. The two curves are representative of the range of corona operation. Figure (8) also shows the variation of the value of the 'convection current' ratio.

In the expression:

$$\bar{v}_p = \bar{v}_\infty + k \bar{E}_{app} + k \bar{E}_{sc}$$

the term  $\bar{v}_\infty$  may be given by the following expression from Shapiro [12].

$$\frac{p_0}{p} = \left[ 1 + \frac{\gamma-1}{2} M^2 \right]^{\frac{\gamma}{\gamma-1}}$$

where:

$$M = \frac{|\bar{v}_\infty|}{a_\infty}$$

For the pressures considered, 8 psig and 14 psig, the respective Mach numbers are 0.832 and 1.02. These correspond to flow speeds, at the injector nozzle exit plane, of 402 m/s at  $P_0 = 22.7$  psia, and 483 m/s at  $P_0 = 28.7$  psia. From the Schlieren photographs the profile of the jet was determined. Assuming continuity, this leads to a prediction of the variation of flow speed in the flow direction.

The increased effectiveness of the high pressure jet may be shown by recalling the slip parameter,  $\delta$ , defined to be the ratio of the particle drift velocity,  $k\bar{E}$ , to the steam jet flow speed. In terms of the non-dimensional electric field output of the computer program,  $\tilde{E}$ ,

the slip parameter is:

$$\delta = \frac{kE_b |\tilde{E}|}{|\bar{v}_\infty|}$$

For a jet with particles well coupled to the flow,  $\delta$  will be less than one. To determine  $\delta$ , the value of  $\tilde{E}$  may be solved for by the computer program. From Eq. (8), the value of  $\rho_{eo}$ , the initial charge density, may be determined. For the low and high pressure jets, this results in 0.0102 and 0.0084 C/m<sup>3</sup>, respectively. Using this density as the program input parameter RHOZRO, an  $|\tilde{E}|$  field distribution may be obtained. This was done for both low and high pressure cases. Other significant parameters used were attractor voltage of 2300 volts, and breakdown field strength of  $3 \times 10^6$  V/m. Figures (9) and (10) are plots of the equipotential surfaces resulting from the computer solution of the low and high pressure jets. Using these results, the variation of  $\delta$  along the centerline of the EGD channel was obtained, and is plotted in Figure (11). The values of  $\delta$  are based on an assumed mobility of  $4 \times 10^{-5}$  m<sup>2</sup>/V-s, a value representative of the range of mobilities of the EGD charged particle [7].

Figure (11) shows that everywhere along the centerline of the EGD channel, with the exception of a single point, the high pressure jet has a lower slip than the low pressure jet. The single point that differs may well be the result of the inaccuracies of the numerical solution. The use of a higher value of mobility would tend to give values of  $\delta$  greater than one. However, if the conjectured distribution of [5] is approximately correct, particles of higher mobility are a small part of the total number of charged particles.



From Eq. (3), the total  $\bar{E}$  field has two contributions. One,  $\bar{E}_{app}$ , is due entirely to the geometry and voltages applied to various parts of the EGD geometry. This can be changed only by a physical change in the geometry or applied voltages. The potential and  $\bar{E}$  field distribution resulting from the geometry alone may be solved for by Laplace's equation. The Laplacian solution represents the potential or  $\bar{E}$  field distribution unaffected by the presence of space charge. Figure (10) is the solution to Poisson's equation, and it shows the added distortion of the distribution due to the presence of space charge, when compared to the Laplacian solution, Figure (12). The added distortion appears in Eq. (3) as the second contribution,  $\bar{E}_{sc}$ , the space charge field. Figure (13) depicts the  $|\tilde{E}|$  field distribution corresponding to the potential distribution of Figure (10). Since the space charge is of the same polarity as the charged particles, their movement is opposed. Elimination or reduction of  $\bar{E}_{sc}$  would enhance charged particle velocity, making the collection easier. Application of a potential to the guard ring is designed to impose an additional external field on the flow. However, if the field overcompensates for the space charge field, and the ring becomes a dominant sink for the charged particles, the purpose of the ring is defeated.

Figure (14) shows the increase in collector current as a result of using the guard ring. The results are shown over a range of voltages at the three positions used. It appears that the position achieving the greatest increase is that of the trailing edge plane coincident with the tip of the collector needle. From Figure (10), this is also the area of greatest space charge distortion, implying that the effects of the ring are concentrated in a small area.



Figures (15), (16) and (17) are graphical computer outputs of potential distribution for a grounded ring, and potentials of 1 and 2 kV. The experimental results also show the proper trend in collector current as ring voltage is increased. That is, the current slowly increases to a broad maximum, and then drops off with further voltage increases, the maximum occurring at about 1 kV.

The computer predicted results of using the guard ring is shown in Figure (18) as a plot of centerline Laplacian  $\tilde{E}$  minus the Poisson  $\tilde{E}$  field. As this difference approaches zero, the particular guard ring distribution approaches the optimum Laplacian distribution. The computer results indicate that the  $\tilde{E}$  field is definitely modified by the presence of the guard ring. The predicted optimum ring voltage, corresponding to maximum collector current, appears to lie between ground and 1 kV. The point common to all curves lies at the midpoint of the ring, and is probably due to the uniformity of the guard ring electric field at this point.

## VII. CONCLUSIONS

The computer program appears to present an accurate picture of the potential and electric field distributions within an EGD device. This is borne out by the computer prediction of experimentally observed trends in EGD channel performance. The 'convection current' ratio,  $I_G/I_T$ , was found to be affected by the steam reservoir conditions. In addition, computer and experimental results agree and show that increased EGD performance can be attained by suitable manipulation of the electric field distribution, and hence of the space charge flow.

The agreement found between analytical and experimental results suggests that the use of the computer program as a design tool, particularly when modeling the space charge flow in a high pressure jet, is feasible.

To be completely general in approach, some further account should be taken of particle mobility. Since the drift velocity appears to be negligible at high pressures, this is especially true when working with particles of high mobility, and/or dielectric jets at low speeds. In this case, the slip parameter could go well above 1, and the present assumption of zero slip will give completely invalid answers. Some preliminary work on determining the mobility range of the charged particles used in these experiments is shown in Appendix D.

## VIII. RECOMMENDATIONS

In addition to the measurement of mobility, the difference equations should be modified to allow for a variable mesh size. Equations of this type may be found in a textbook such as Reference [10]. This will allow a greater generality in selecting geometries to be studied, and will also do away with a great deal of the error involved in discrete jet profile approximation. It will almost certainly mean greater computer storage requirements.

As a design tool, the program can be used to determine the optimum guard ring geometry and voltage. From the curves of Figure (18), the solutions for the various voltages diverge from the optimum in the vicinity of the collector needle. A guard ring geometry capable of affecting this divergence, yet maintaining the distribution of the remainder of the 1 kV curve, would appear to be an improvement.

It should also be possible to use the program as a design tool to optimize both injector nozzle and collector geometries. A nozzle geometry allowing for the use of smaller guard ring sizes may allow for more effective guard ring performance, yet forestall breakdown. An optimum collector geometry may exist which will allow for greater charge collection efficiency resulting simply from the geometry, rather than by flow manipulation to achieve the higher collector currents.

Other applications outside the EGD field may also exist. For instance, the program may be used to study the region of space charge known as an electrode 'sheath' which divides a neutral plasma and an electrode. Also, Reference [4] covers a study of EGD control of separated flow. This study may be extended through use of the program to determine optimum electrode geometries for control.

## APPENDIX A: NORMALIZATION PROCEDURE

The vector form for Poisson's equation is:

$$\nabla^2 \phi = - \frac{\rho_e}{\epsilon_0}$$

After expanding in cylindrical coordinates:

$$\frac{1}{r} \frac{\partial \phi}{\partial r} + \frac{\partial^2 \phi}{\partial r^2} + \frac{\partial^2 \phi}{\partial z^2} = - \frac{\rho_e}{\epsilon_0}$$

By defining:

$$R = \frac{r}{h} ; \quad A = \frac{\phi}{V} ; \quad Z = \frac{z}{h}$$

where:

$h$  = characteristic channel length of EGD geometry

$V$  = maximum potential

and substituting into the various terms:

$$\frac{1}{r} \frac{\partial \phi}{\partial r} = \frac{1}{h(\frac{r}{h})} \frac{V \frac{\partial(\frac{\phi}{V})}{\partial(\frac{r}{h})}}{h \frac{\partial(\frac{r}{h})}{\partial r}} = \frac{V}{h^2 R} A_R ; \quad \frac{\partial^2 \phi}{\partial r^2} = \frac{V \frac{\partial^2(\frac{\phi}{V})}{\partial(\frac{r}{h})^2}}{h^2 \frac{\partial(\frac{r}{h})^2}{\partial r^2}} = \frac{V}{h^2} A_{RR}$$

similarly for  $\frac{\partial^2 \phi}{\partial z^2}$ . By combining and clearing the left side:

$$\frac{1}{R} A_R + A_{RR} + A_{ZZ} = - \frac{h^2 \rho_0}{V \epsilon_0}$$

Defining:

$$C = \frac{h^2 \rho_{eo}}{V \epsilon_0} ; \quad \rho = \frac{\rho_e}{\rho_{eo}}$$

The normalized equation becomes:

$$\frac{1}{R} A_R + A_{RR} + A_{ZZ} = - C \rho$$

Similarly for the two-dimensional form of Poisson's equation. By defining:

$$X = \frac{x}{h} \quad ; \quad Y = \frac{y}{h}$$

The two dimensional form becomes:

$$A_{XX} + A_{YY} = -C\rho$$

The electric field may be normalized by defining:

$$\tilde{E} = \frac{E}{E_b}$$

where:  $\tilde{E} \equiv$  the normalized value of  $E$

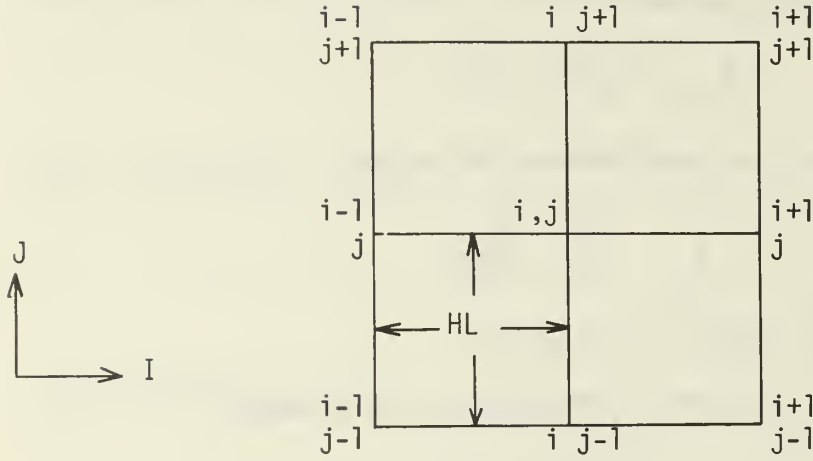
$E_b \equiv$  the dielectric breakdown field strength

from:  $E = -\nabla\phi$

$$\frac{hE}{V} = -\frac{h}{V} \nabla\phi = -\nabla A$$

then:  $\tilde{E} = -\frac{V}{hE_b} \nabla A$

## APPENDIX B: FINITE DIFFERENCE EQUATION DERIVATION



Knowing the value at any point in the mesh, the value at another point, nearby, may be found by means of a Taylor series. By writing the series in the J direction, expressions for  $A_{i,j+1}$  and  $A_{i,j-1}$  may be found. These are:

$$A_{i,j+1} = A_{i,j} + HLA'_{i,j} + \frac{HL^2}{2!} A''_{i,j} + \frac{HL^3}{3!} A'''_{i,j} + \dots \quad (1)$$

$$A_{i,j-1} = A_{i,j} - HLA'_{i,j} + \frac{HL^2}{2!} A''_{i,j} - \frac{HL^3}{3!} A'''_{i,j} + \dots \quad (2)$$

Solving for  $A'_{i,j}$ , neglecting higher order terms where primes indicate the derivative with respect to the direction of interest:

$$A'_{i,j} = \frac{A_{i,j+1} - A_{i,j-1}}{2HL} \quad (3)$$

To determine the finite difference equation for the second partial derivative, add (1) and (2). This results in:

$$A_{i,j+1} + A_{i,j-1} = 2 A_{i,j} + HL^2 A''_{i,j} + \dots$$



Solving for  $A_{i,j}''$ , again neglecting higher order terms:

$$A_{i,j}'' = \frac{A_{i,j+1} + A_{i,j-1} - 2 A_{i,j}}{HL^2} \quad (4)$$

By writing the series in the I direction, solving for values of  $A_{i+1,j}$  and  $A_{i-1,j}$ , and adding the resulting equations, the second derivative in the I direction may be determined. The resulting equation is:

$$A_{i,j}'' = \frac{A_{i+1,j} + A_{i-1,j} - 2 A_{i,j}}{HL^2} \quad (5)$$

By combining (3), (4), and (5), and solving for  $A_{i,j}$ , a finite difference form of Poisson's equation in axisymmetric form is obtained. The axisymmetric form is:

$$A_{i,j} = \frac{1}{4} \left[ HL^2 C_p + A_{i+1,j} + A_{i-1,j} + A_{i,j+1} + A_{i,j-1} + \frac{HL}{2R} (A_{i,j+1} - A_{i,j-1}) \right] \quad (6)$$

For points along a boundary where the normal derivative is equal to zero, the equations for the value on the boundary may be derived in the same manner and cast in the form of second order forward or backward difference equations. Assuming  $(i,j-1)$  is on the boundary of interest, the series equations become:

$$A_{i,j+1} = A_{i,j-1} + 2 HLA_{i,j-1}' + \frac{4 HL^2}{2!} A_{i,j-1}'' + \frac{8 HL^3}{3!} A_{i,j-1}''' + \dots (7)$$

$$A_{i,j} = A_{i,j-1} + HLA_{i,j-1}' + \frac{HL^2}{2!} A_{i,j-1}'' + \frac{HL^3}{3!} A_{i,j-1}''' + \dots \quad (8)$$

Multiplying (8) by 4 and subtracting from (7):

$$A_{i,j+1} - 4 A_{i,j} = -3 A_{i,j-1} - 2 HLA_{i,j-1}' + \dots$$

Neglecting higher order terms:

$$A'_{i,j-1} = \frac{A_{i,j+1} - 4 A_{i,j} + 3 A_{i,j-1}}{-2 HL} \quad (9)$$

Setting the normal derivative equal to zero, and solving for  $A_{i,j-1}$ :

$$A_{i,j-1} = 1.333 A_{i,j} - .333 A_{i,j+1} \quad (10)$$

The successive over-relaxation method (SOR) uses previously calculated values to speed up convergence. For a point inside the mesh, the final difference equation becomes:

$$A_{i,j}^{n+1} = A_{i,j}^n + \frac{\omega}{4} \left[ HL^2 C_p + A_{i+1,j}^n + A_{i-1,j}^{n+1} + A_{i,j+1}^n + A_{i,j-1}^{n+1} + \frac{HL}{2R} (A_{i,j+1}^n - A_{i,j-1}^{n+1}) - 4A_{i,j}^n \right] \quad (11)$$

For a point on a boundary of zero normal derivative, the equation becomes:

$$A_{i,j-1}^{n+1} = A_{i,j-1}^n + \omega \left[ 1.333 A_{i,j}^n - .333 A_{i,j+1}^n - A_{i,j}^n \right] \quad (12)$$

## APPENDIX C: PROGRAM DESCRIPTION

The computer program is designed to solve a finite difference form of Poisson's equation, either in axisymmetric or two-dimensional form, at each node defined by a uniform square mesh covering the geometry to be studied. In order to do this, the program must be able to do the following:

1. Determine which finite difference equation is to be solved.

This is a function of the geometry and the node position within the mesh.

2. Determine and store charge distribution at each node.
3. Solve the difference equation and store the answer.
4. Determine when a solution to the problem has been attained.
5. Provide the results in an easily interpreted form.

The program is made up of two major parts: preparation and calculation, and output of results. In general at each point in the EGD channel defined by the uniform mesh, there exists a charge density and a potential. The charge density may be zero. This can be the case inside of the jet, as well as outside. The voltage may either be the result of an electrode presence or a potential surface between electrodes. If the voltage is due to an electrode presence, this value will remain constant, otherwise it will vary as a function of the charge density. The program must be able to make this differentiation. In all, the program must know the potential at a point, the charge density, and whether the point defines a portion of an electrode. In order to simplify the program coding, the program stores all values of potential in one array, "A". The values of charge density are stored in a separate array, "G", of the same size.

This array is also used to store all information required to determine whether the potential is that of an electrode, the potential description value (PDV), or is to be changed as a function of the charge density. This can be done since a point of constant potential will be an electrode, and a charge density cannot exist at the same point.

The program determines convergence of the solution method by comparing answers from the (n+1)st iteration with those obtained on the (n)th iteration. This will reveal the maximum change in potential as a result of the iteration. If the maximum is less than some designated value, the iterative procedure is stopped. This method requires storage for the answers generated by the (n)th iteration. These are stored in array "B". The value of the potential resulting from the previous solution is required for the SOR method. This value is supplied from array "B". Hence the variables required for the solution of the finite difference equation are taken from three separate sources. A superposition of arrays "A" and "B" describes the complete situation at any node within the EGD channel.

The program has been written for use on an IBM 360/67 Computer System. The output is in both printed and plotted form. The plotting was accomplished on the CALCOMP Model 765. The program consists of the following subroutines:

SUBROUTINE NAME	PURPOSE
MAIN (Main Program)	General coordination of preparation and calculation phase and output phase.
GSPRD	Calculates cloud radius. Determines charge density at each point, and stores in "G" array.
GENFIL	Reads geometry input.
CALC1	Calculates potential. Determines $\vec{E}$ field components and modulus.

WRITER	Prints values of potential, $\vec{E}$ field and $\vec{E}$ field components, determined in CALC1.
CLVL	Determines lines of constant potential and constant $\vec{E}$ field to be plotted.
FLOP	Orients arrays to coincide with output labeling convention.
OUTPUT	General coordination of output phase.
CONTUR	Coordination of labeling and plotting of graph, and preparation for plotting results. Modified NPGS Computer Library subroutine, which allows the superposition of three sets of contours on one plotted output.

All data, except the electrode geometry is read in under NAMELIST control. This requires a special format for all cards, but provides for a more flexible means of handling the data in that there are no fixed fields in which the variables must appear, nor must the arrangement coincide with that of the NAMELIST statement.

The first data card required by MAIN is the card denoting the appearance of the data group. It has the format, starting in column 2; &PARAM. PARAM is the NAMELIST name. The first column of all data cards is ignored. Each data item may be separated from the following by a comma. However, no comma must appear between the NAMELIST name and first data item. More than one data item may appear on a card. Each data item is in one of the two forms below.

1. "Variable name" = FORTRAN constant
2. "Array name" = a set of FORTRAN constants, separated by constants [13].

The variables read in are listed below. The first five are explained with the help of the representative geometry in Figure ( 2).



NAME	TYPE	DESCRIPTION
NATRAD	I*4	Mesh column number of attractor inner radius. This is the point defined as (6,3). Then the value assigned to NATRAD is 3.
NBLOCK	I*4	The number of discrete points, lines, or blocks of points required to completely describe the charge distribution or geometry of the problem. For the figure shown, the attractor ring may be defined by a block of points, a line and a single point. The corona needle, and collector needle may each be defined by two lines of points. In addition, if it is assumed that the collector needle collects all the charge, a block of points can be used to define the area within the dielectric jet where in no charge exists. Thus, for the geometry and charge distribution of the problem shown, NBLOCK = 8.
NDLPNT	I*4	Mesh row position of corona needle tip. For the geometry shown, NDLPNT = 4.
NDLRAD	I*4	Mesh column number of corona needle centerline. For geometry shown, NDLRAD = 1.
NOZPOS	I*4	Mesh row number of attractor exit plane. For the geometry shown, NOZPOS = 6.
BRKDOWN	R*4	Breakdown field strength of dielectric gas. (volts/meter)
CONVER	R*4	Characteristic channel length of EGD geometry. (centimeters)
DELU	R*4	Value compared with maximum difference between iterations. If the maximum difference is less than desired value of DELU, convergence of the iterative scheme is signaled.
GAPPOT	R*4	Maximum fixed potential covered by the mesh. In general, the attractor will be at the maximum potential.
IH	I*4	Desired height of output plot measured along longitudinal coordinate ( $IH \leq 15$ )
IW	I*4	Desired width of output plot measured along radial coordinate ( $IW \leq 9$ )
NCOLS	I*4	Number of mesh columns ( $NCOLS \leq 61$ ).
NDIMEN = 0	I*4	Indicates problem is a two-dimensional geometry in constant area channel.
= 1	I*4	Indicates problem is axisymmetric.
NGLOSS = 0	I*4	No charge density decrease accounted for in the conversion section other than by charge cloud spreading.

NGLOSS = 1	I*4	Some loss mechanism (recombination, etc.) and cloud spreading will be accounted for in determining charge cloud densities.
NL	I*4	Number of potential contours desired in plotted output ( $NL \leq 20$ ).
NLI	I*4	Number of $\tilde{E}$ field contours desired in plotted output ( $NLI \leq 20$ ).
NOLINE = -1	I*4	Only potential and $\tilde{E}$ field contours will be plotted.
= 0	I*4	Only physical geometry (fixed potential) points will be plotted.
= 1	I*4	Physical geometry will be superimposed on contour plot.
NROWS	I*4	Number of mesh rows ( $NROWS \leq 81$ )
RHOZRO	R*4	Charge density at exit plane of attractor (coulombs/cubic meter)

The last card in the NAMELIST signals the end of the list. The format is &END. Again the symbol ampersand must appear in column 2 of the data card.

The jet radius and charge density distribution are calculated by subroutine GSPRD according to the charge profile given by statement numbered 35. In the case of a two-dimensional geometry, only the charge distribution is calculated, as the jet is assumed to fill the entire two-dimensional channel. The charge density will remain constant throughout the flow in the channel, unless some charge loss mechanism is introduced, signaled by the value of NGLOSS. The jet profile and charge distribution for a geometry with an off center corona needle is also determined by GSPRD.

Subroutine GENFIL is used to input the specific values of potential and charge density or PDV. This is accomplished with the help of the variable NBLOCK, which is used as a DO-LOOP parameter. The loop causes the program to read the exact number of data cards defined by NBLOCK. Since each block defined by NBLOCK contains points of common value, the entire block can be represented by a single data card. The format for these data cards is 4I3,2F12.4

The variables read in by GENFIL are:

NAME	TYPE	DESCRIPTION
NI1	I*4	Mesh row number of beginning of line or block.
NI2	I*4	Mesh row number of end of line or block.
NJ1	I*4	Mesh column number of beginning of line or block.
NJ2	I*4	Mesh column number of end of line or block.
AV	R*4	Normalized potential common to all points encompassed by NI1, NI2, NJ1 and NJ2.
GV	R*4	EITHER: Normalized charge density common to all mesh points encompassed by NI1, NI2, NJ1 and NJ2. OR: Potential description value (PDV) if the defined points are at a fixed potential.

An arbitrary value of 99. is the PDV used to describe a point of fixed potential. No arithmetic operations will be carried out at this point. Note also that  $NI1 \leq NI2$ , and  $NJ1 \leq NJ2$ , since these variables are the beginning and end of a DO-LOOP. In the case of a point,  $NI1 = NI2$  and  $NJ1 = NJ2$ . In the case of a line of points, either  $NI1 = NI2$  or  $NJ1 = NJ2$ , depending on the orientation of the line. The values assigned to the above variables to describe the representative geometry are shown below:

NI1	NI2	NJ1	NJ2	AV	GC	Corresponding to
1	6	5	15	1.0	99.	NBLOCK 1
5	6	4	4	1.0	99.	NBLOCK 2
6	6	3	3	1.0	99.	NBLOCK 3
1	4	1	1	0.0	99.	NBLOCK 4
1	3	2	2	0.0	99.	NBLOCK 5
14	20	1	1	-0.1	99.	NBLOCK 6
15	20	2	2	-0.1	99.	NBLOCK 7
17	20	3	6	0.5	0.0	NBLOCK 8

At the same time that the values of AV and GV are being loaded into the appropriate arrays, the coordinates of those points with a PDV of 99. are being converted into plotter pen position coordinates to aid in

plotting the output requested by NOLINE. The pen position coordinates are stored in the appropriate vectors, XLIN and YLIN for later use during the output phase.

Subroutine CALC1 solves the appropriate form of the finite difference equations, depending on the geometry variable NDIMEN, and location of the point in question. In addition, once the potential distribution has been calculated, CALC1 determines the  $\tilde{E}$  field, and the longitudinal and radial components of the  $\tilde{E}$  field. The value of the  $\tilde{E}$  field and its components are normalized with respect to the breakdown field strength of the dielectric, BRKDOWN, while the values of potential are normalized with respect to the maximum fixed potential, GAPPOT. The derivation of the normalization of  $\tilde{E}$  is shown in Appendix A, which gives:

$$\tilde{E} = - \frac{V}{hE_b} \nabla A$$

The characteristic EGD geometry length 'h' is read into the program by the value of the variable CONVER. Defining:

$$\$ALPH = \frac{V}{hE_b}$$

$$|\tilde{E}| = \$ALPH |-\nabla A|$$

The value of the constant \$ALPH is calculated by MAIN, and is passed to CALC1 as a calling argument. By normalizing  $\tilde{E}$  in this manner, a quick glance at the results will show whether or not the electric fields produced will exceed the dielectric breakdown strength. The results of CALC1 are printed by subroutine WRITER.

For the graphical output of the results, subroutine OUTPUT coordinates the various plotting subroutines required. The remainder of the required data cards are read in by subroutines OUTPUT under NAMELIST



control. The first data card is &TABL, starting in column 2. The variables in NAMELIST TABL are read into two vectors, TABLE and LTG, in the format:

"Array name" = a set of FORTRAN constants, separated by a comma.

The format for the elements of TABLE is TABLE( ) = '-----', where (-) indicates a card column available for a data item. This format prepares the data to be used in labeling the graphical output. The variables read in are:

NAME	TYPE	DESCRIPTION
TABLE (1)	R*8	Nozzle radius in centimeters
TABLE (2)	R*8	Initial charge density in C/m <sup>3</sup>
TABLE (3)	R*8	Maximum fixed potential (GAPPOT)
TABLE (4)	R*8	Dielectric permittivity
TABLE (5)	R*8	Breakdown field strength of dielectric
TABLE (6)	R*8	Characteristic length modeled

The elements of the vector LTG can be used to construct a grid for the plotted output, label it and the plotted contours. The vector LTG is typed LOGICAL \* 1. The variables read into the vector LTG are:

LTG (1)	L*1	.TRUE.	All exterior contour segments and those interior contour segments which represent a local maximum will be labeled.
		.FALSE.	Omits labeling option.
LTG (2)	L*1	.TRUE.	Request tic marks and corresponding scale values one inch apart on the exterior frame of the contour graph.
		.FALSE.	Omits "tic" option.
LTG (3)	L*1	.TRUE.	Request a one inch by one inch straight line grid to superimposed on the contour graph.
		.FALSE.	Omits the grid option.

Again, the last card signals the end of the NAMELIST. The format is:

&END

with the symbol ampersand in column 2 of the data card.



## APPENDIX D: MOBILITY MEASUREMENTS

The apparatus used to investigate the mobility of the charged particles is shown in Figure (19). This consists of a fine Monel steel grid concentric with a stainless steel cylinder. The EGD process under investigation involves the transport of negatively charged particles. Hence if a voltage is applied to the grid and varies from zero to some value below ground, the grid will repel or pass negatively charged particles. If at the same time, the outer cylinder is maintained at ground, those particles passed by the grid will be accelerated across the gap, giving a noticeable variation in current flow due to the charge arriving at the outer cylinder. From the definition of drift velocity:

$$\bar{v} = k \bar{E}$$

and assuming that the  $\bar{E}$  field is uniform:

$$\bar{v} = k \frac{V}{l} ,$$

where  $l$  is the spacing between the grid and outer cylinder. But since:

$$\bar{v} = \frac{l}{t}$$

The mobility may be determined by:

$$k = \frac{l^2}{tV}$$

By varying the frequency with which the grid voltage changes and ensuring that the waveform is a square wave, the entire range of mobility possessed by the charged particles can be estimated, assuming that mobility is proportional to the electric field between the cylinders. This is because at the lower frequencies, all particles will be affected, while

at the higher frequencies, or small  $t$ , inertia effects will deter all but the smallest or most highly charged particles from completing their journey. This is similar to the method of Rutherford as outlined by Darrow [14].

The measurements leading to an approximation of the mobility distribution were made at a reservoir pressure of eight psig, over a wide range of temperatures, 238 - 296°F. After steam flow conditions had stabilized, i.e., proper pressure and constant temperature, the device was inserted into the EGD channel to such a position that it was axially symmetric with the steam jet, but not touching. This was done to keep condensation on the grid to a minimum. The grid was powered by a square wave generator while the outer ring was maintained at ground. See Figure (18) for a schematic of the setup. Current from the ring was fed to an oscilloscope for observation. It was found that the ring current varied considerably as the charged particles arrived from the Monel grid. This variation existed over a range of frequencies. At high temperatures, 296°F, the range of current excitation appeared to be concentrated at a single point, 2.1 kHz. As the temperature of the steam was decreased, the range increased considerably, until at 238°F, the current excitation existed from an upper frequency of 5 kHz to a lower frequency of .5 kHz.

At 296°F, the mobility corresponding to 2.1 kHz is  $4.15 \times 10^{-4} \text{ m}^2/\text{V-s}$ , while at 238°F, the mobility range runs from  $1 \times 10^{-3} \text{ m}^2/\text{V-s}$  to  $1 \times 10^{-4} \text{ m}^2/\text{V-s}$ . The range of mobilities appears to arise from both the ability of large particles to move at low frequencies and the lower temperature producing a greater distribution in particle size. However, further work remains to be done to determine both size distribution and further definition of the mobility distribution.

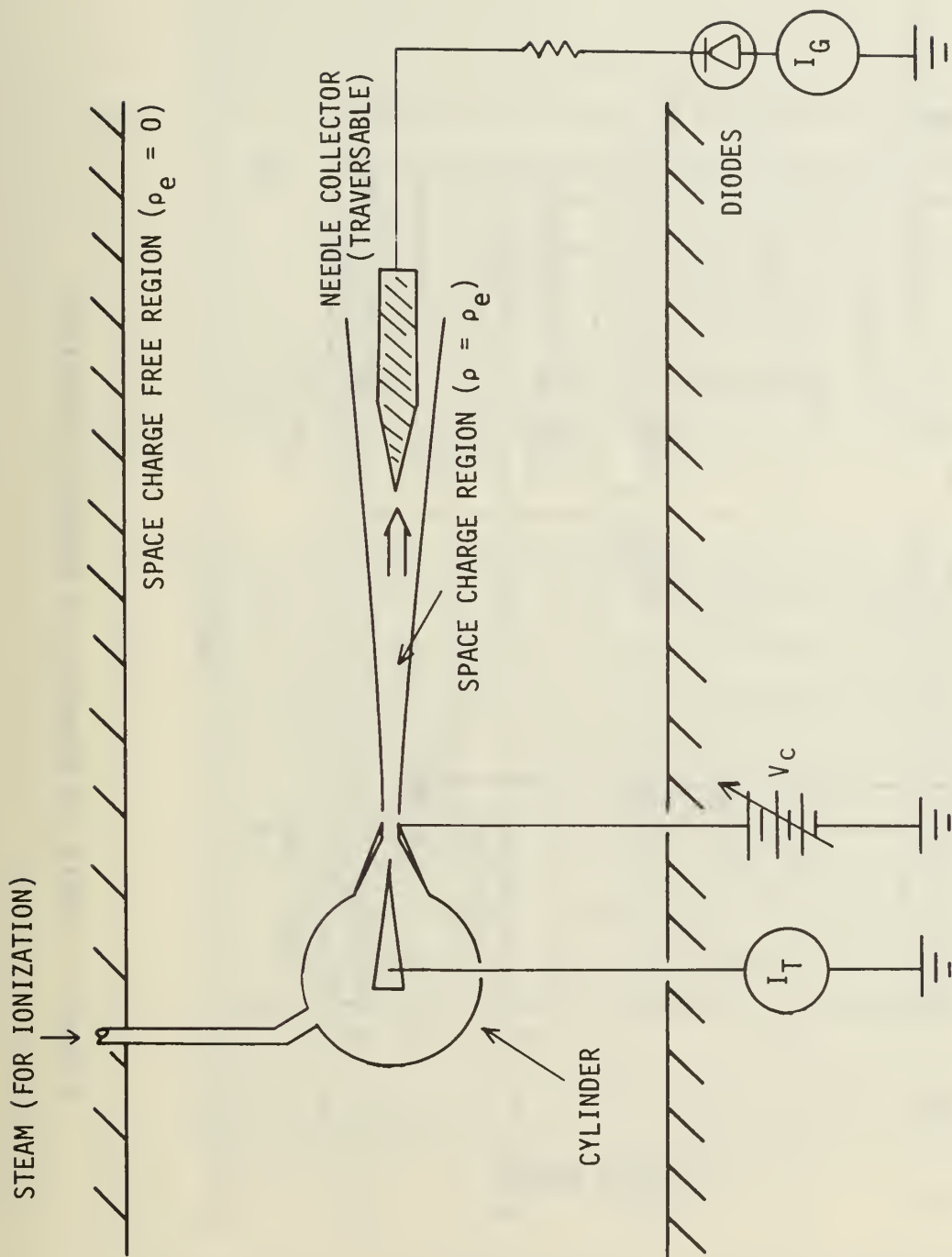


Figure 1. EGD Generator Schematic.

Figure 2. Sample EGD Geometry and Boundary Conditions.

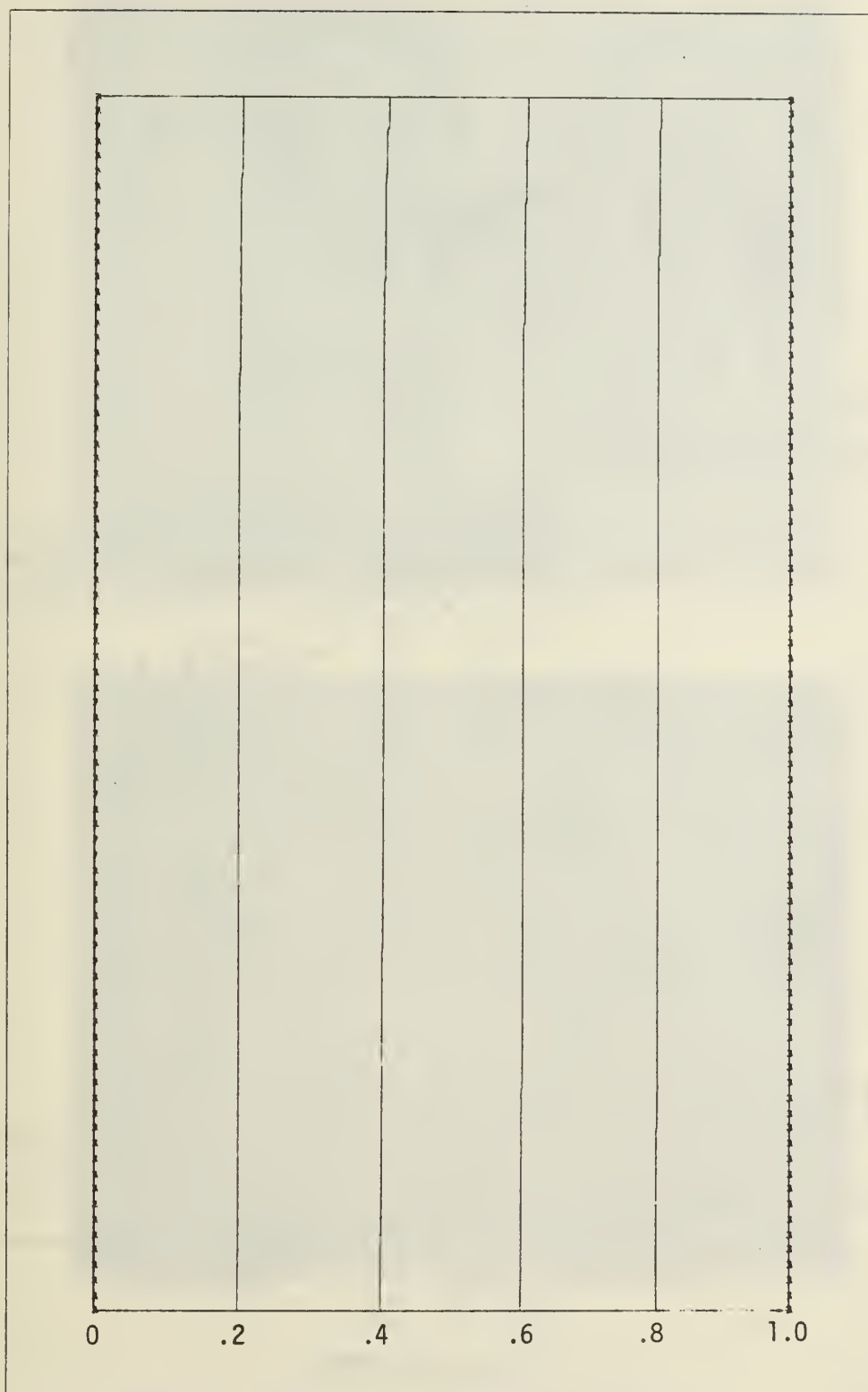
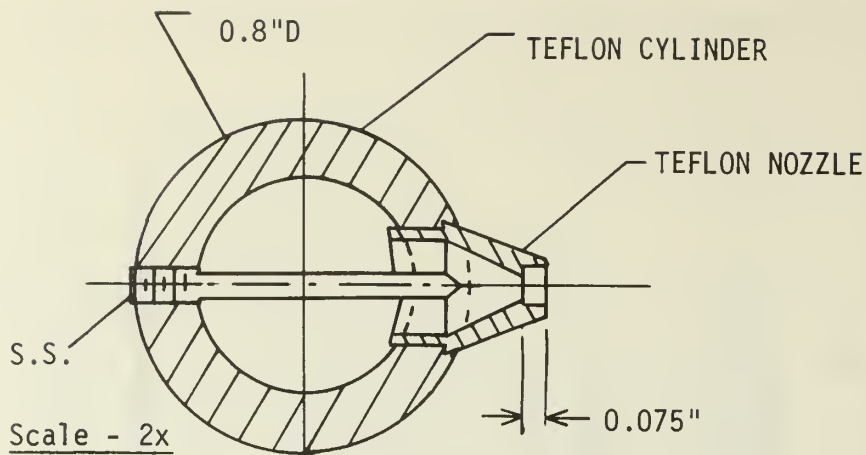
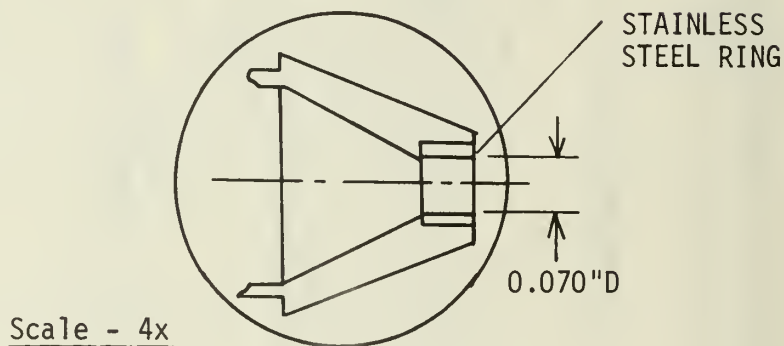


Figure 3. Computer Prediction of Parallel Electrode Normalized Potential Distribution at Breakdown.



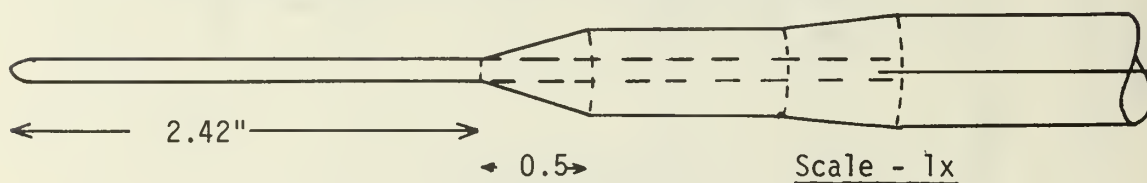


Adjustable Spacing Between  
Corona Needle and Ring



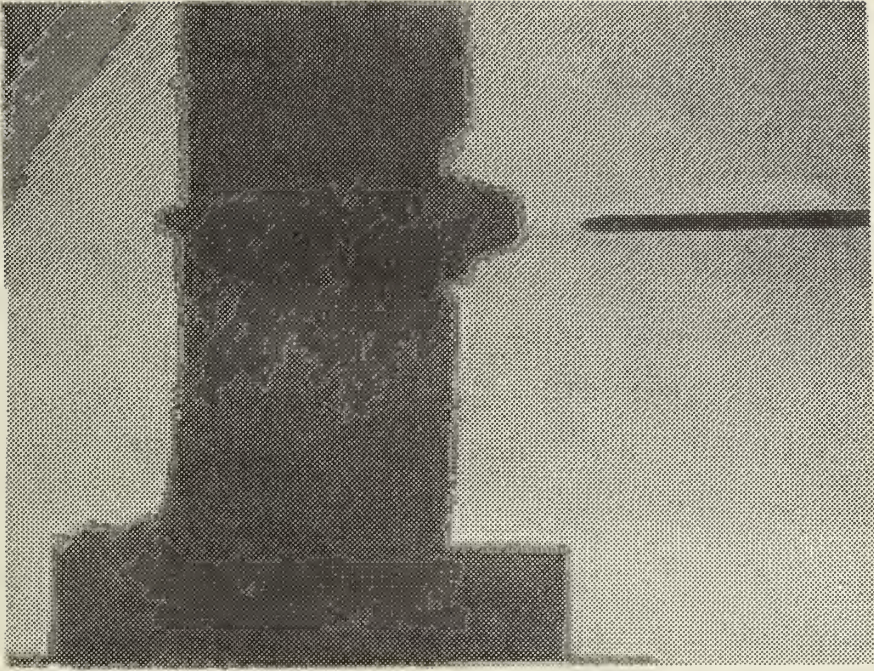
### AEROSOL INJECTOR

#316 STAINLESS STEEL ROD - 0.062" DIAMETER

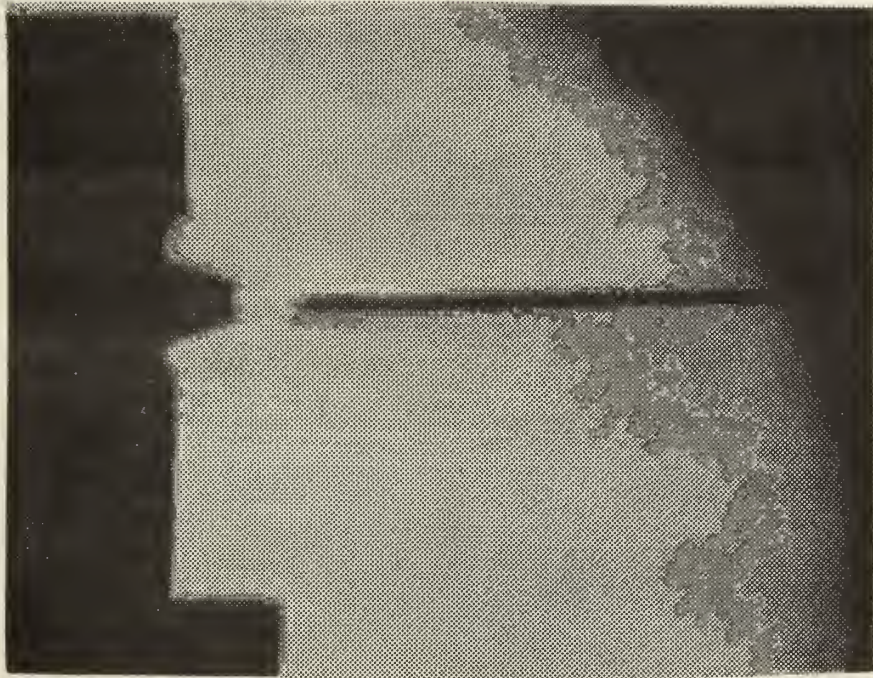


### COLLECTOR PROBE

Figure 4. Aerosol Injector and Collector Probe.



$P_0 = 8 \text{ psig}$



$P_0 = 14 \text{ psig}$

Figure 5. Steam Jet Schlieren Photographs

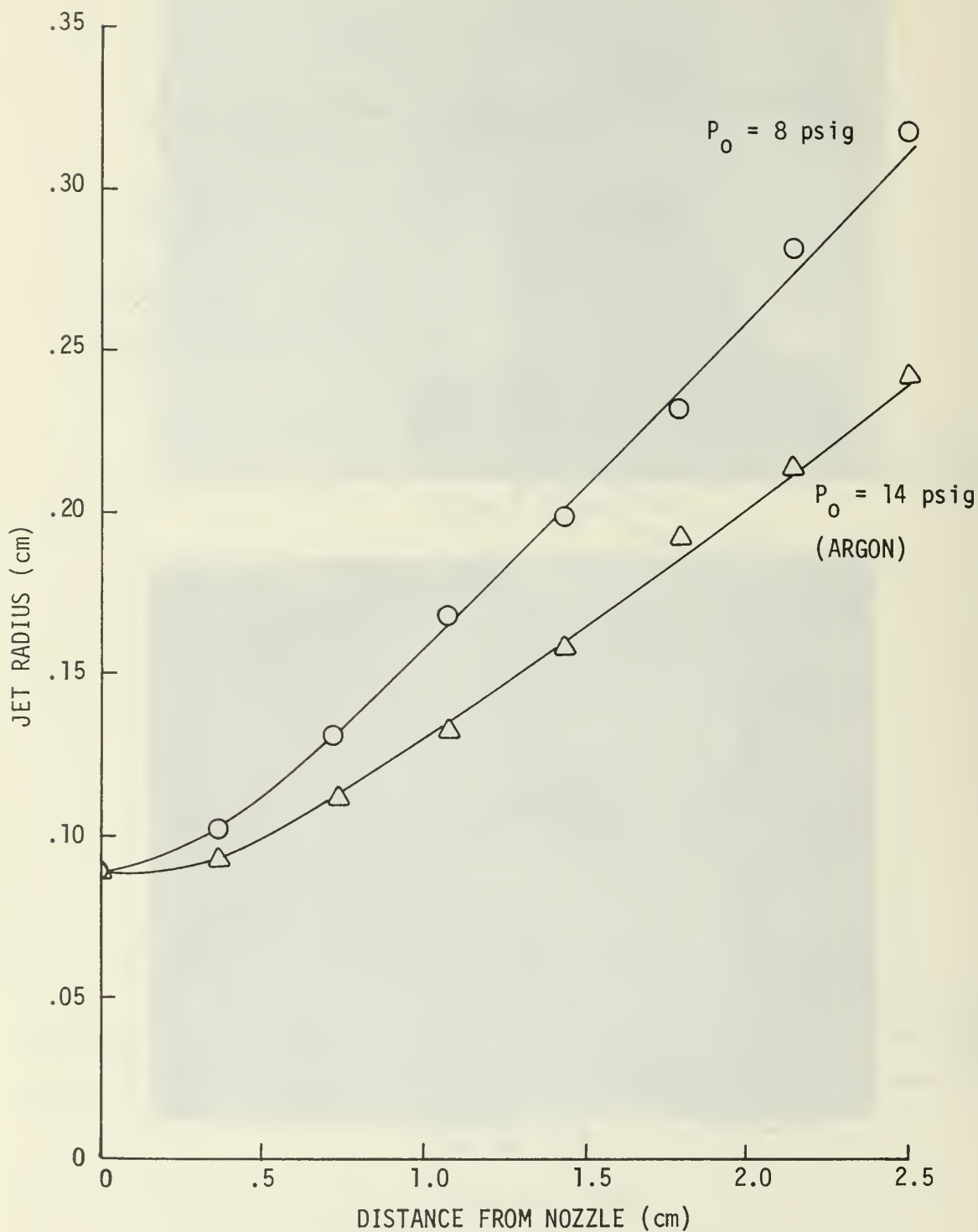


Figure 6. Steam Jet Profile (Axisymmetric).



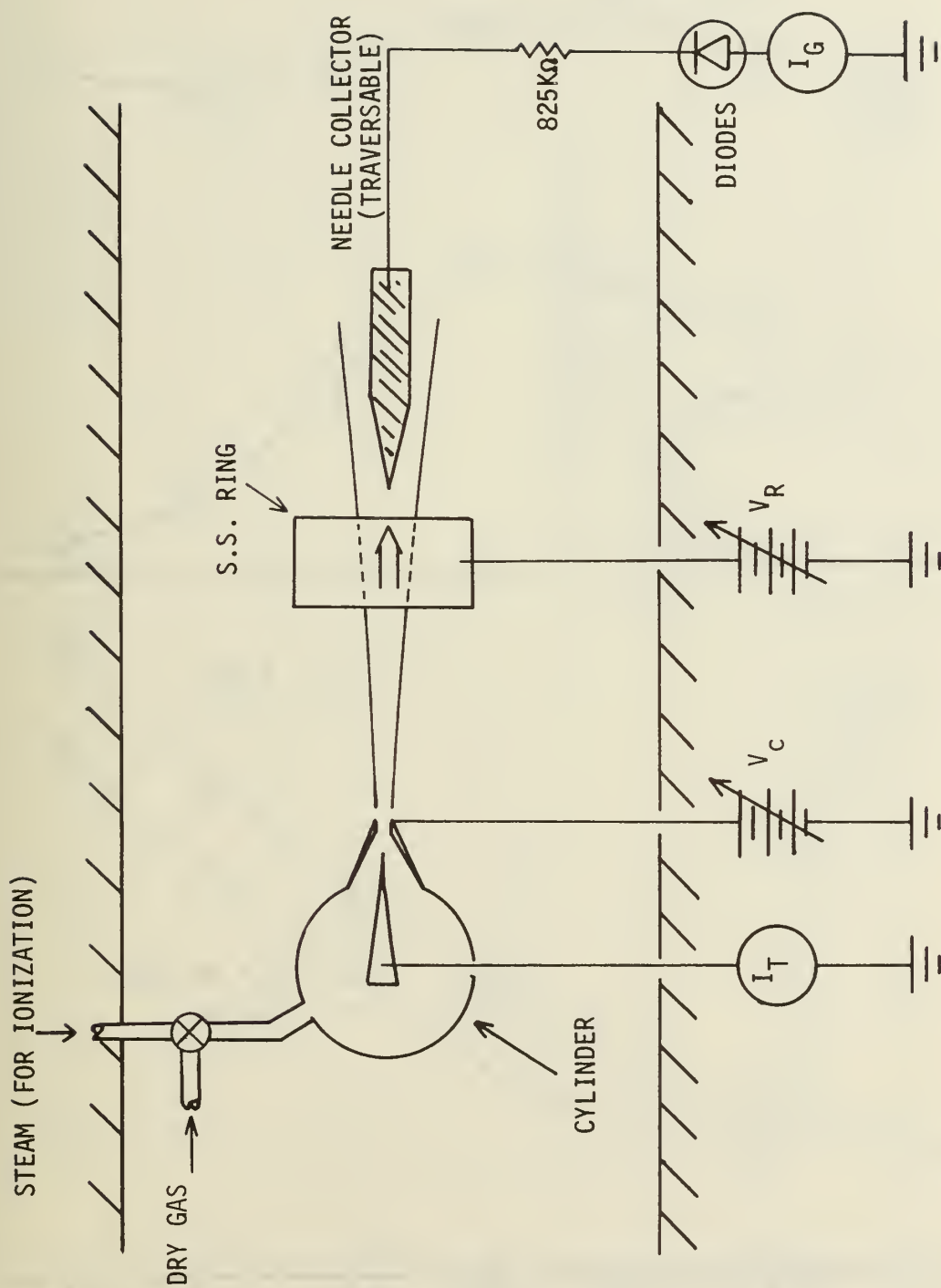


Figure 7. Guard Ring Schematic.

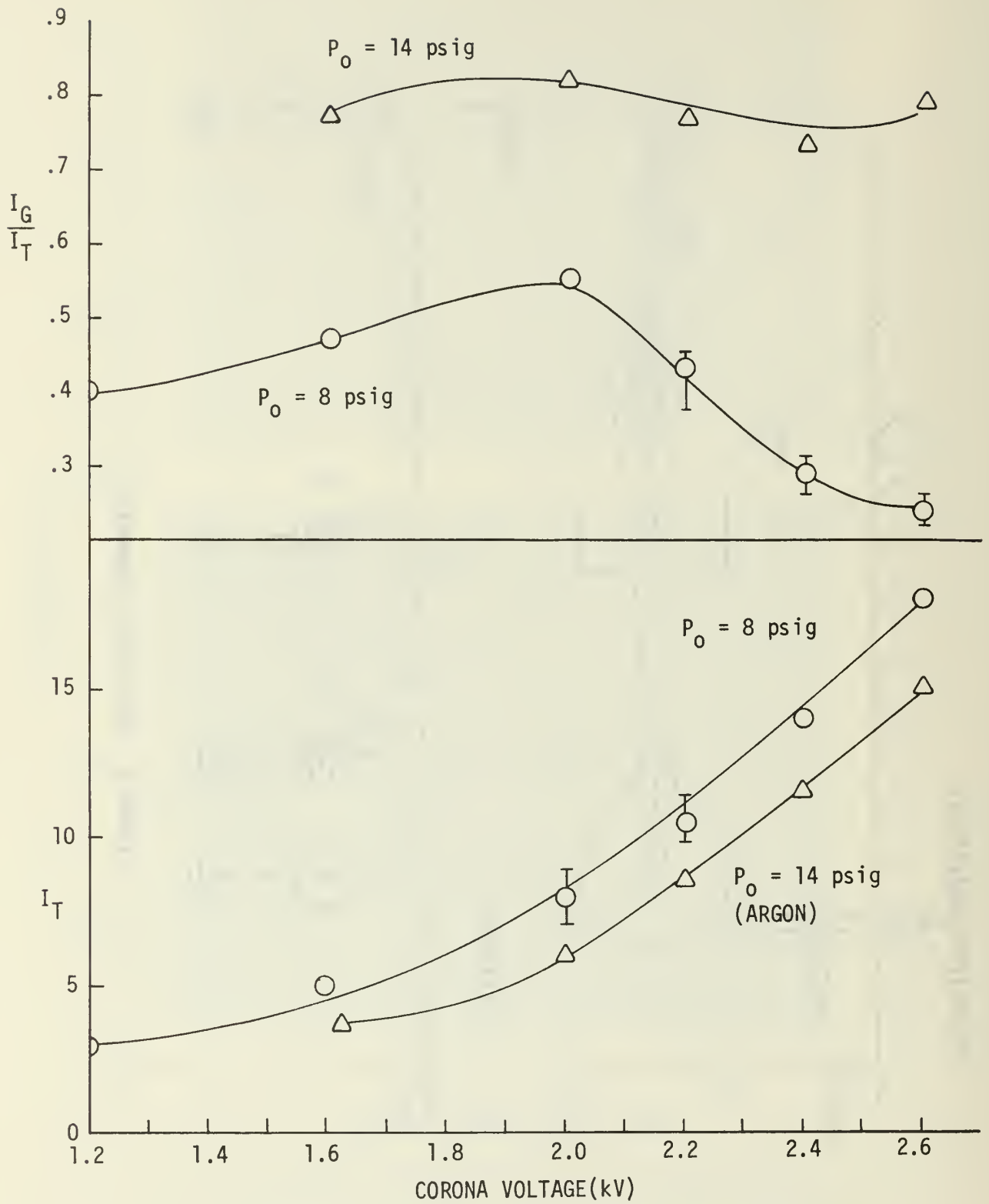


Figure 8. Corona Current and Convection Current Efficiency Ratio vs. Corona Voltage.



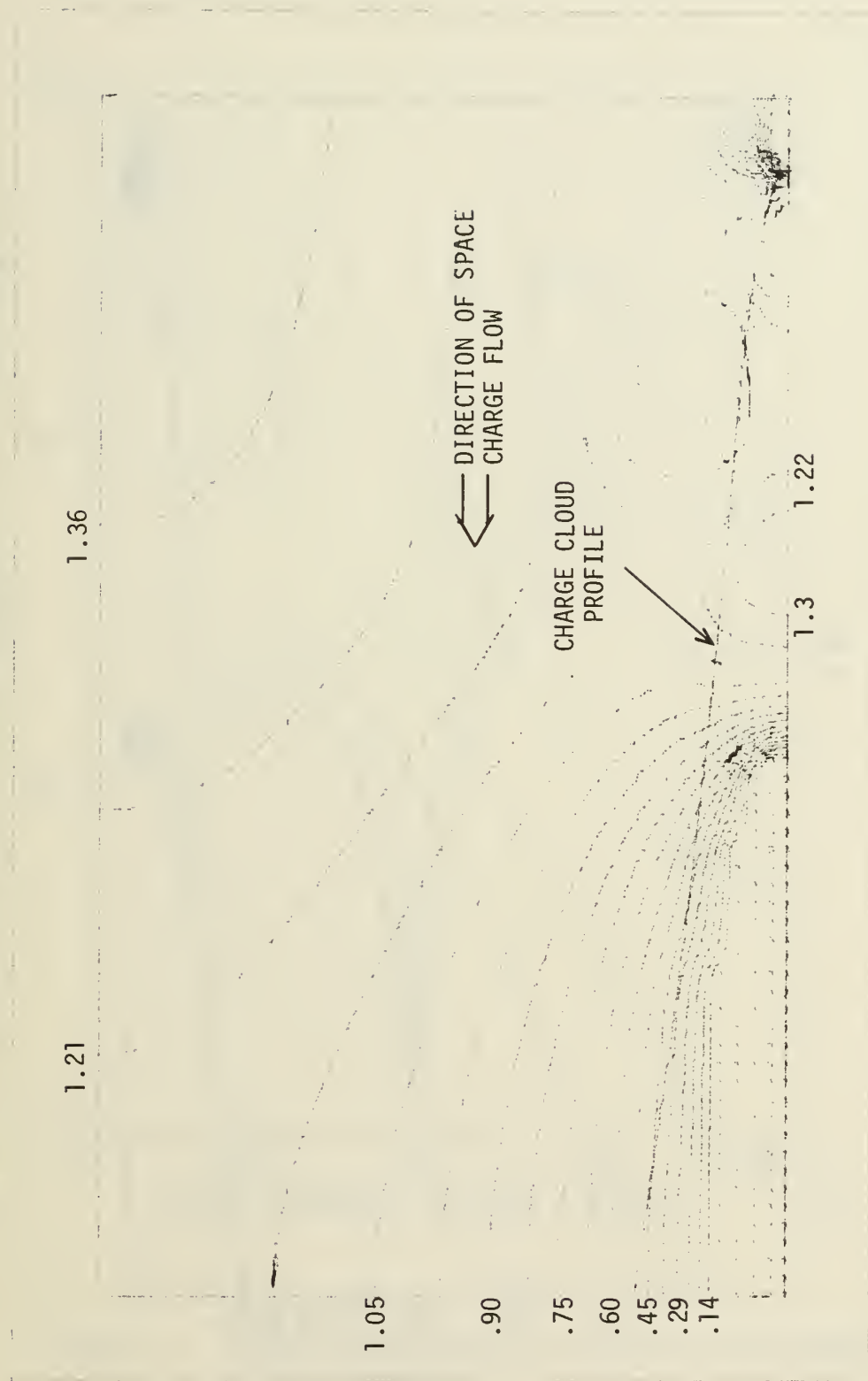


Figure 9. Potential Distribution,  $P_0 = 8$  psig,  $\rho_{e0} = .0103 \text{ C/m}^3$ .

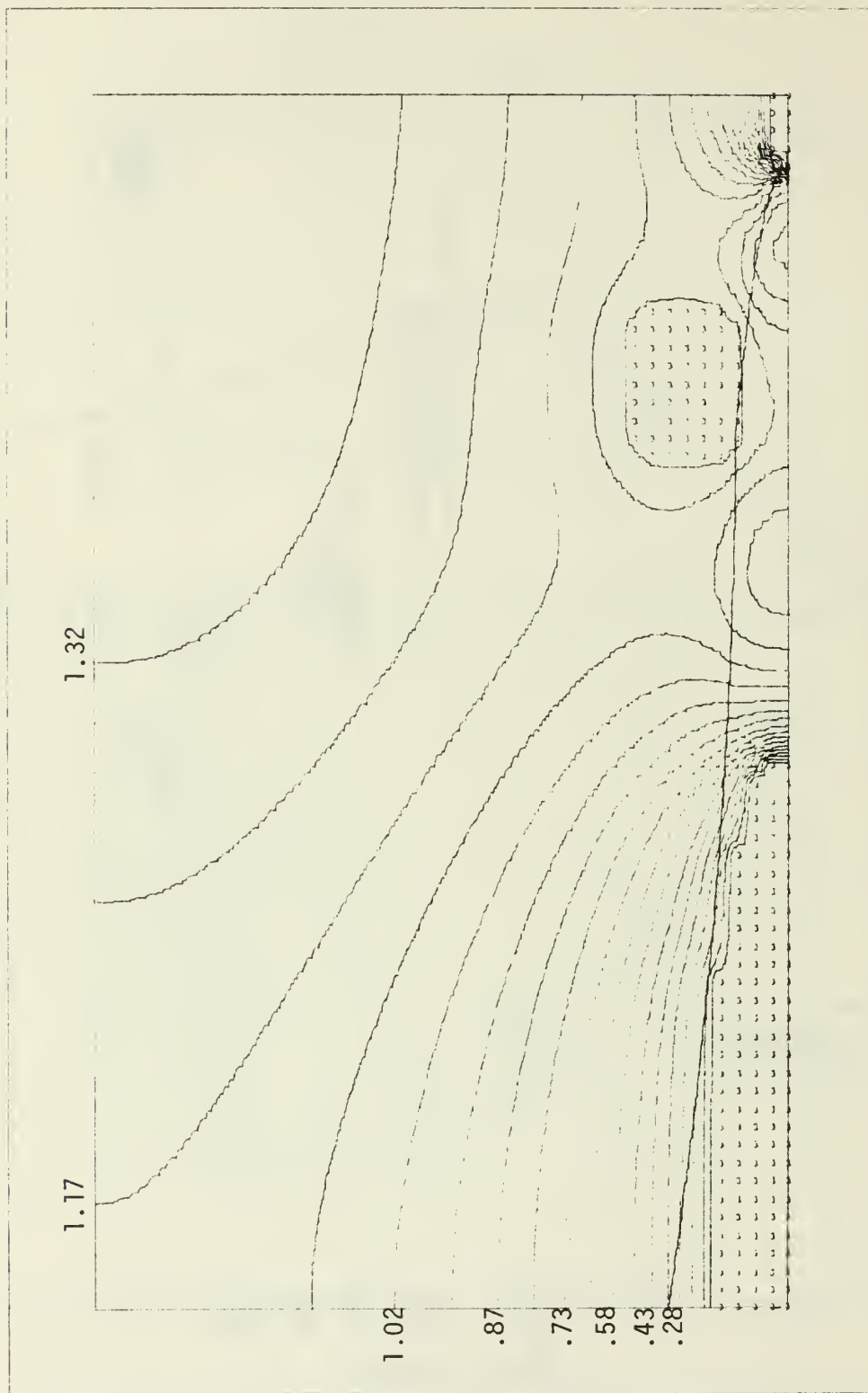


Figure 10. Potential Distribution,  $P_o = 14$  psig,  $\rho_{eo} = .0084 \text{ C/m}^3$ .

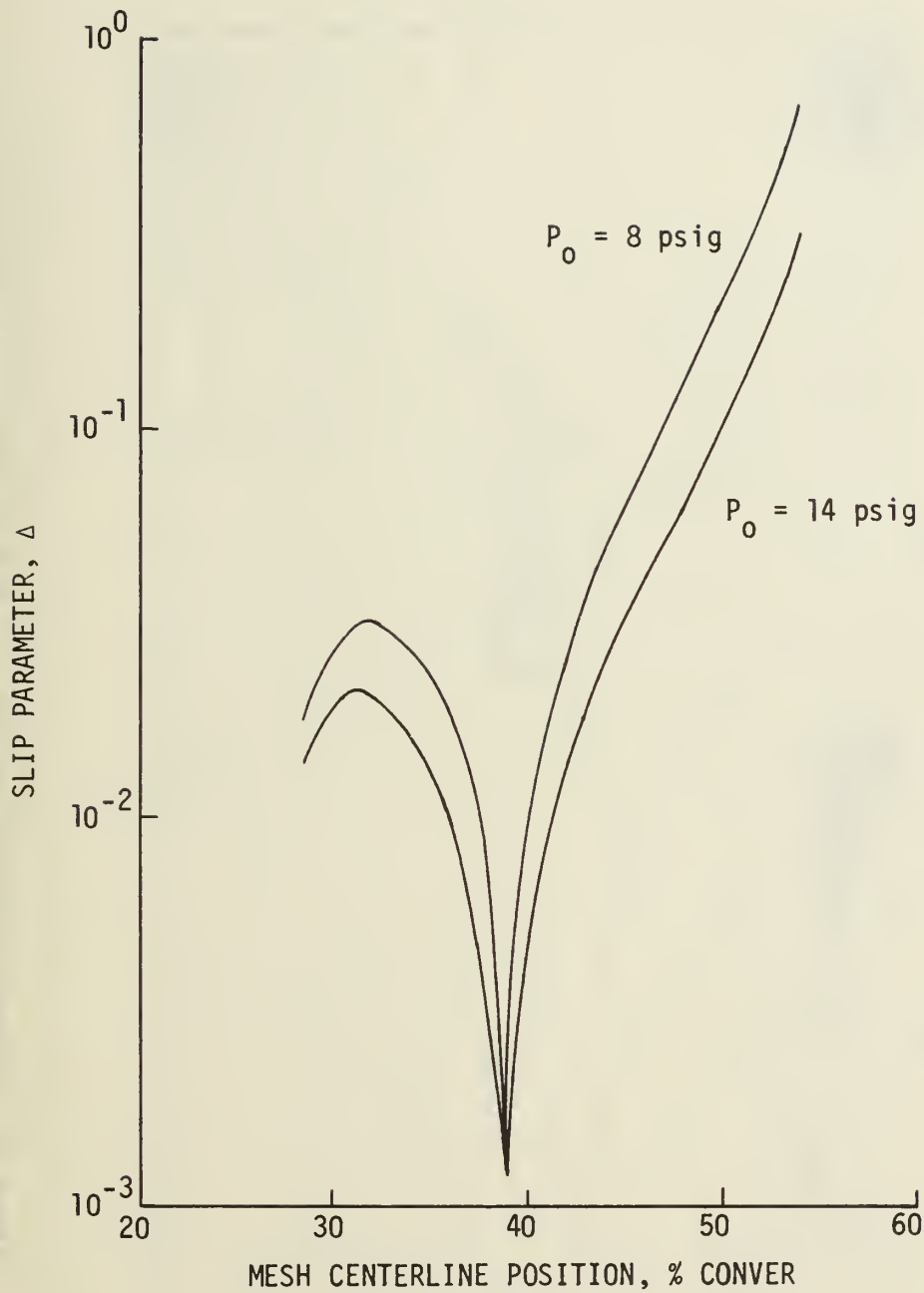


Figure 11. Computer Prediction of Centerline Distribution of Slip Parameter.

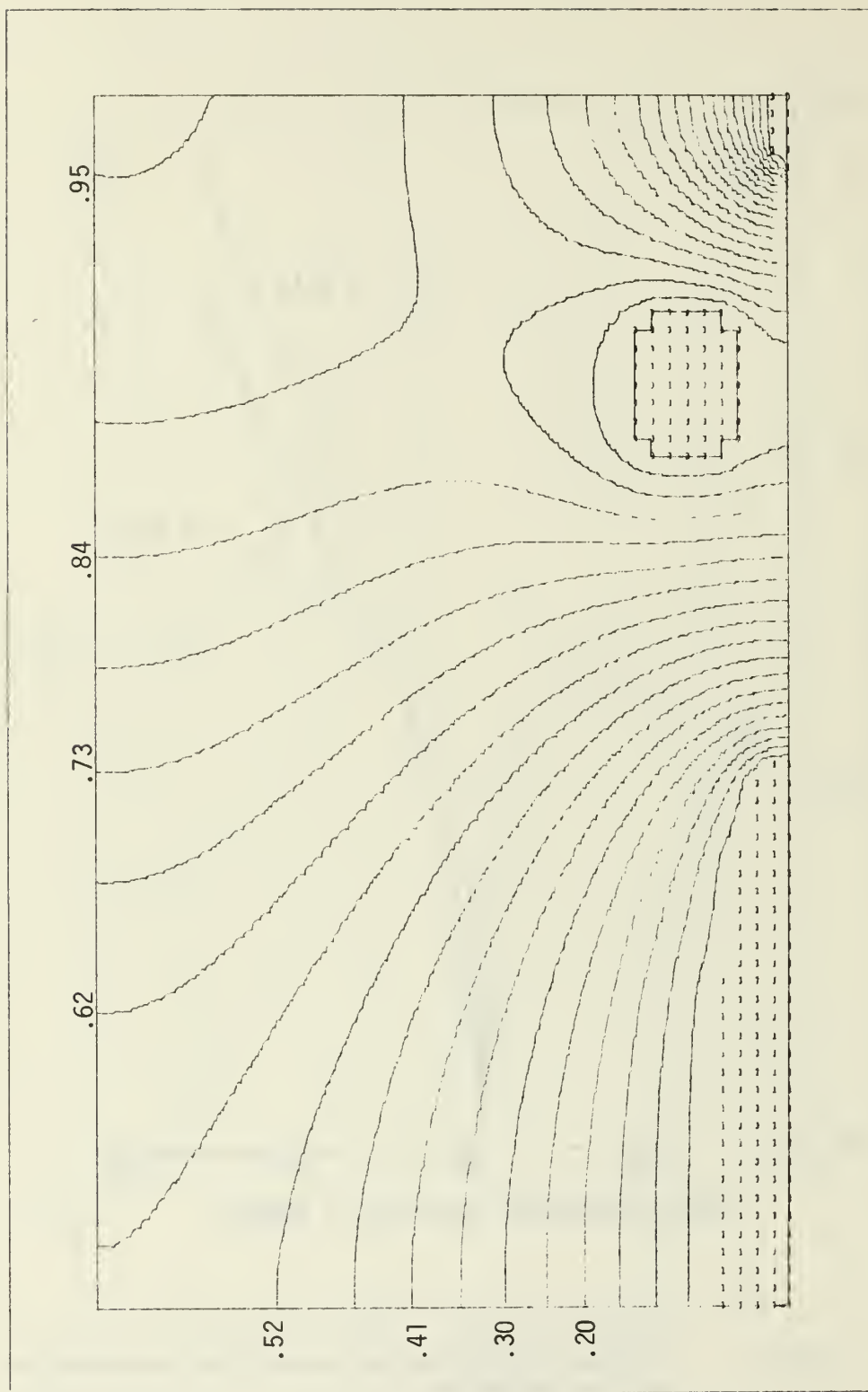


Figure 12. Potential Distribution,  $\rho_{eo} = 0.0 \text{ C/m}^3$  (Laplacian).

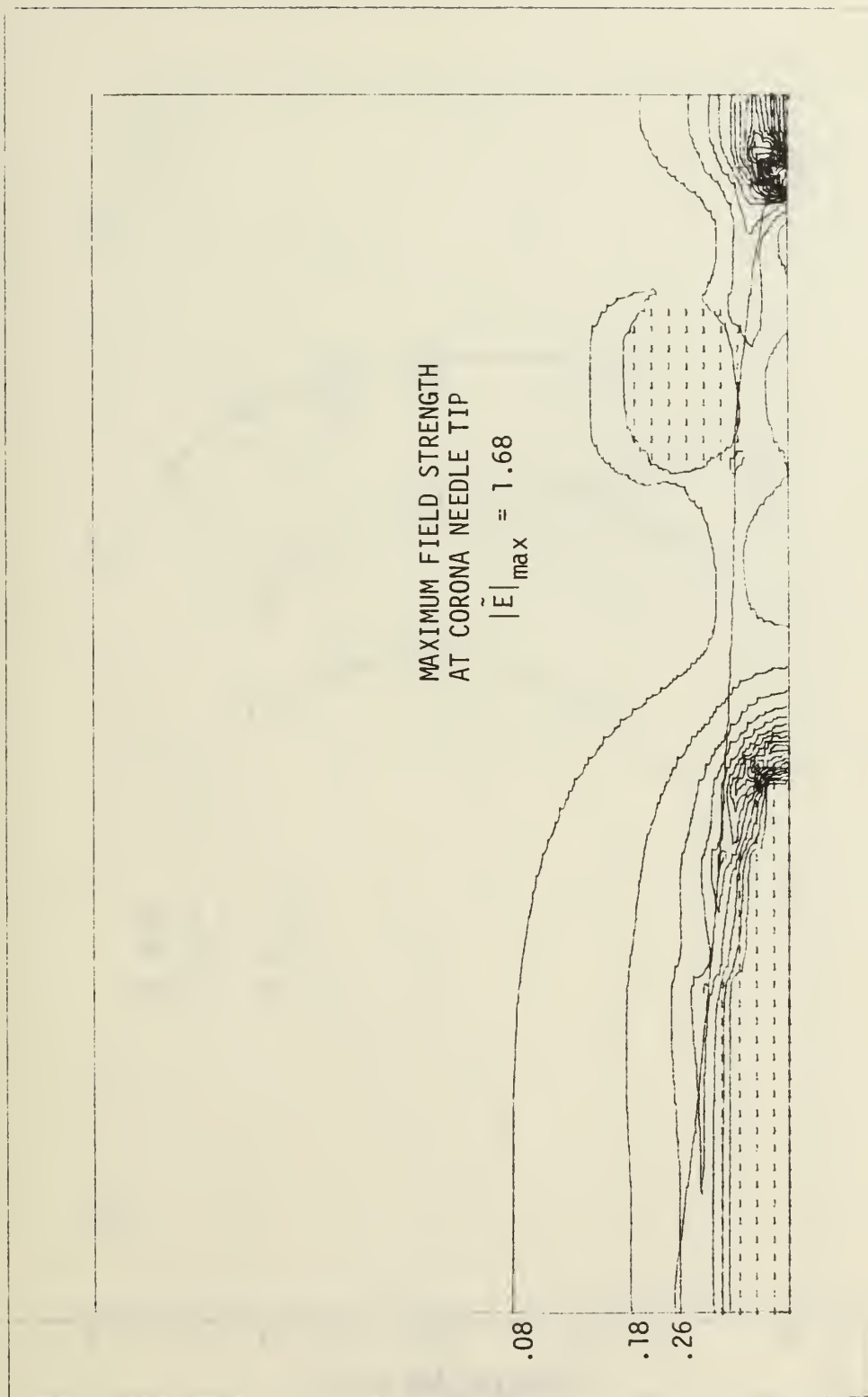


Figure 13. Electric Field Distribution,  $P_0 = 14$  psig,  $\rho_{eo} = .0084 \text{ C/m}^3$ .



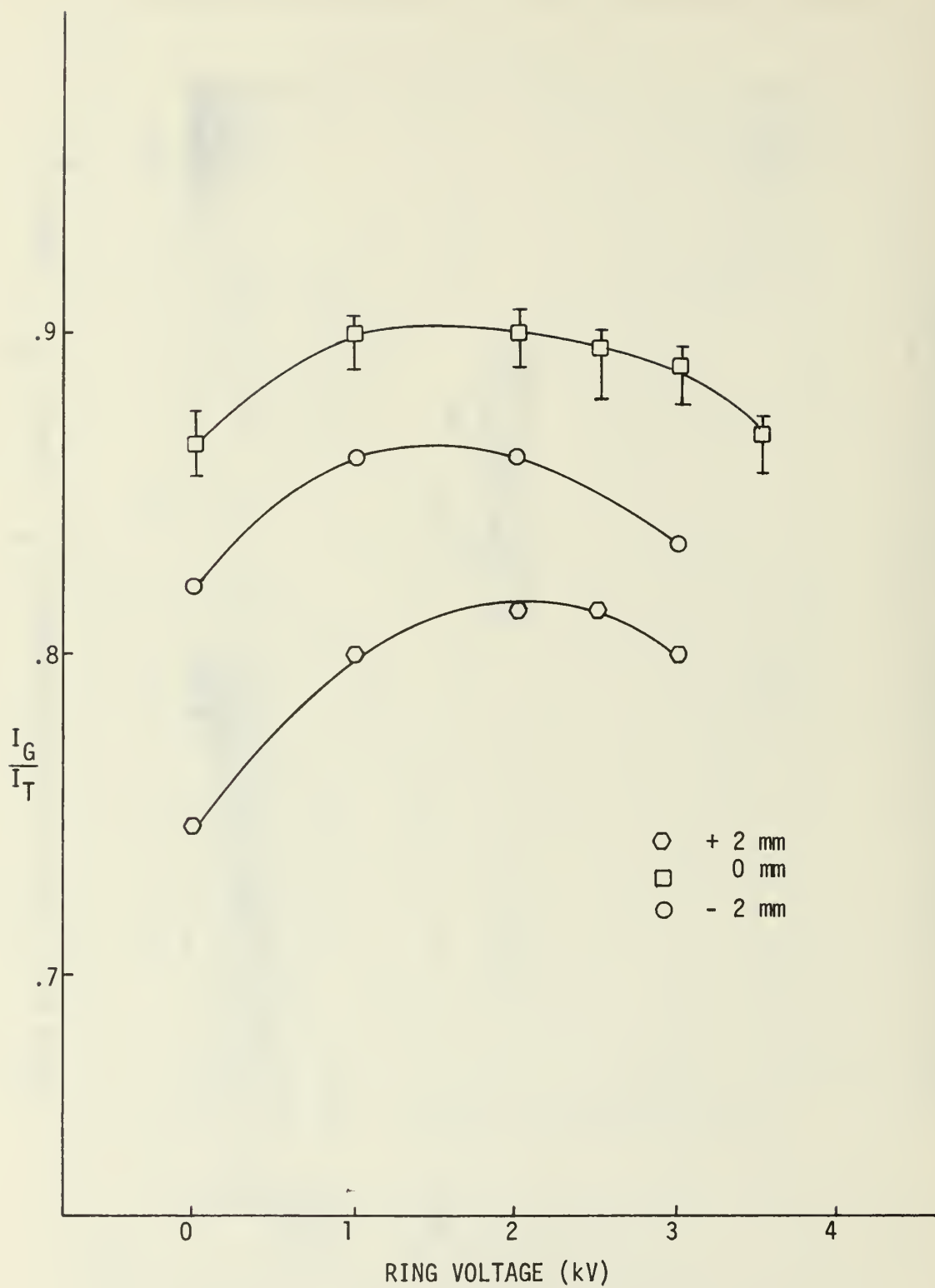


Figure 14. Collector Current Increase Due to Guard Ring.

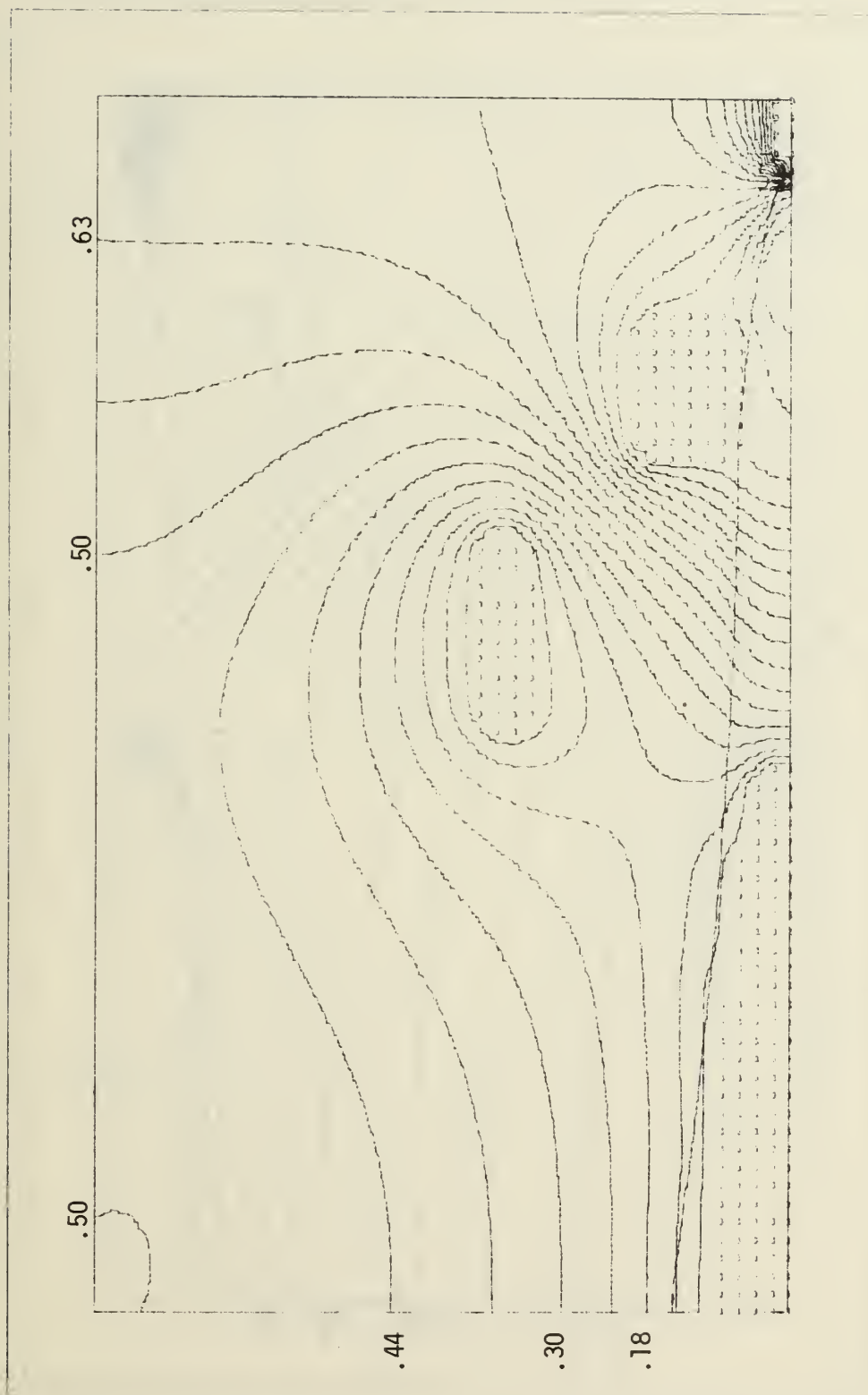


Figure 15. Potential Distribution,  $P_o = 14$  psig, Guard Ring Voltage = 0.

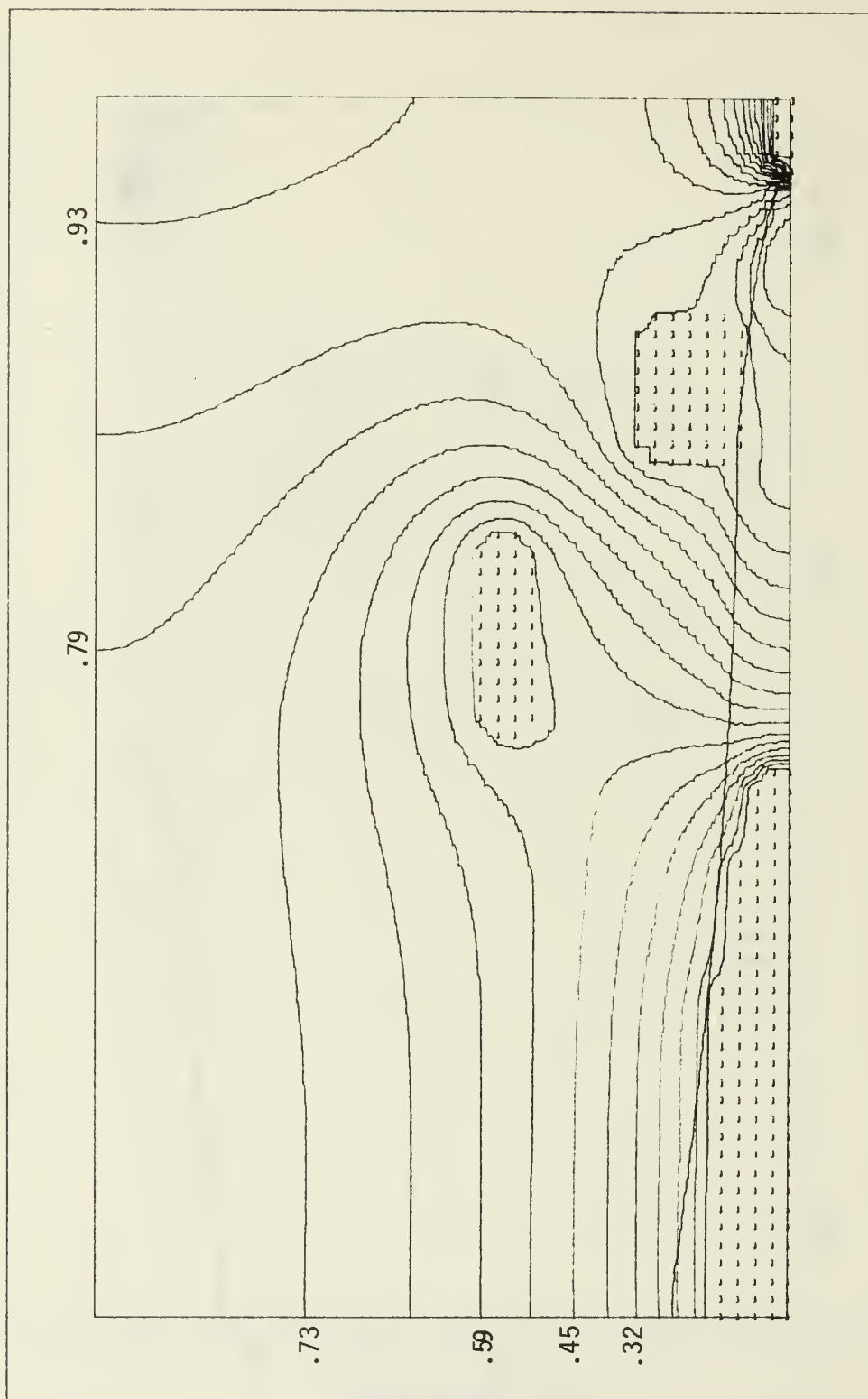


Figure 16. Potential Distribution,  $P_0 = 14$  psig, Guard Ring Voltage = 1 kV.

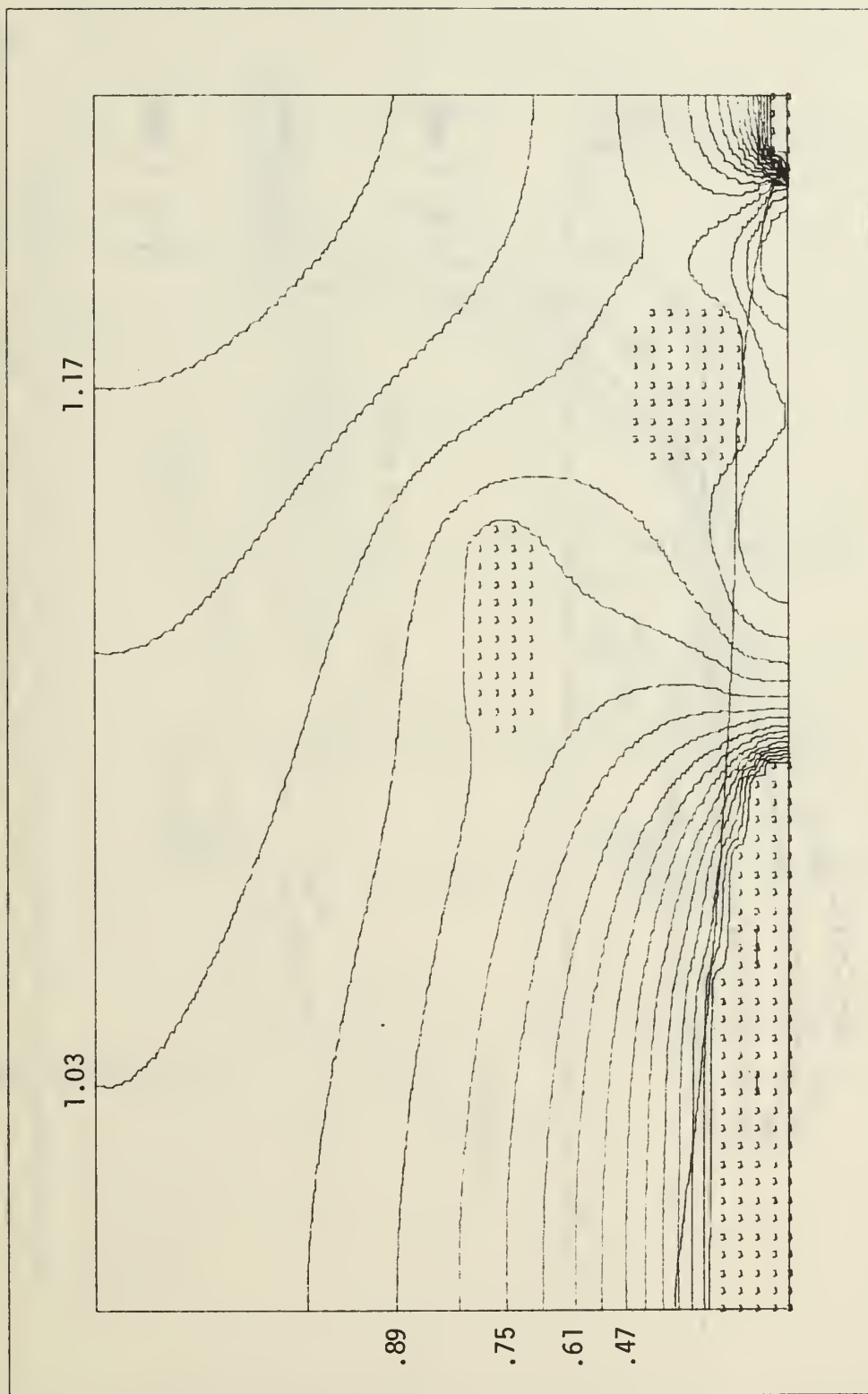


Figure 17. Potential Distribution,  $P_0 = 14$  psig, Guard Ring Voltage = 2 kV.

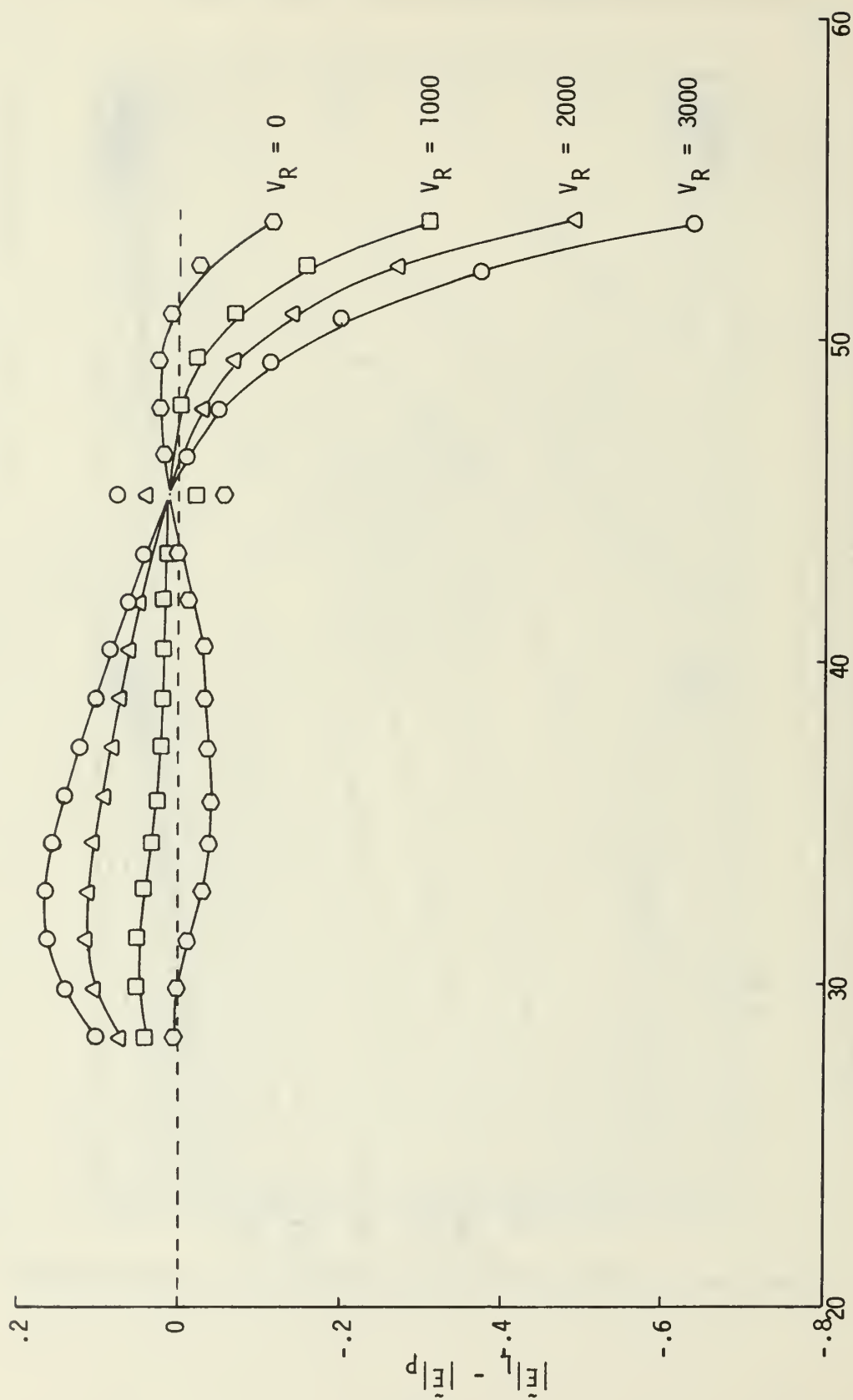


Figure 18. Comparison Between Laplacian  $|\tilde{E}|$  Field Distribution and Poisson  $|\tilde{E}|$  Field Distribution Using the Guard Ring.



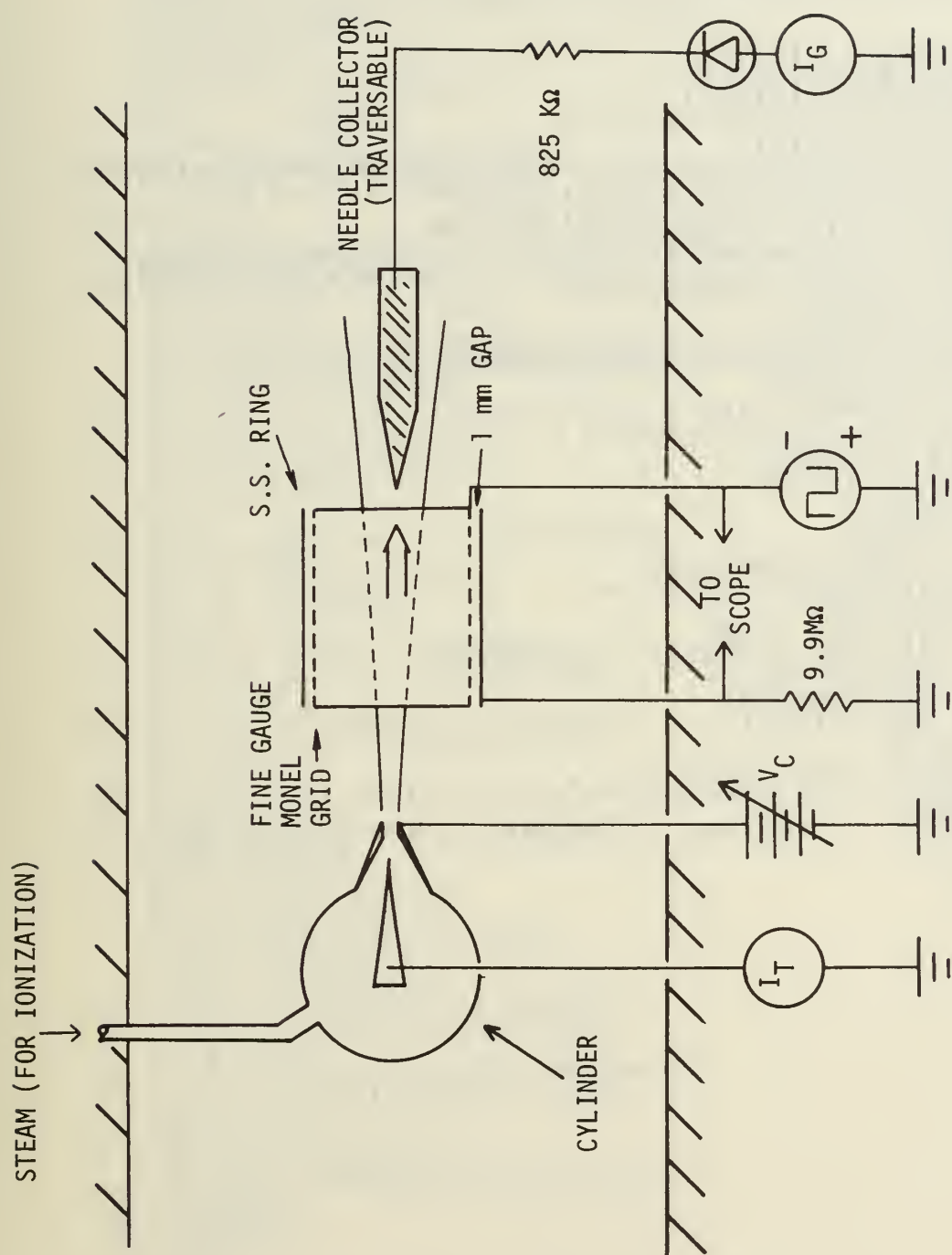


Figure 19. EGD Mobility Measuring Schematic.

# COMPUTER PROGRAM

```

COMMON/BL1/A(81,61)
COMMON/BL2/B(81,61)
COMMON/BL3/G(81,61)
COMMON/BL4/NOLINE,N1,IW,IH
COMMON/BL5/R(81)
COMMON/BL6/NATRAD,RHOZRO,PRMTVT,GAPPOT,BRKDWN,CONVER,
1 NOZPOS,NGLOSS,NROWS,NCOLS,DELU,NBLOCK,NL,NL1,HL
COMMON/BL10/NDIMEN,NDLPNT,NDLRAD
COMMON/BL11/XLIN(4000),YLIN(4000)
NAMELIST/PARAM/NATRAD,RHOZRO,PRMTVT,GAPPOT,BRKDWN,
1 CONVER,NOZPOS,NGLOSS,NROWS,NCOLS,NDIMEN,DELU,NBLOCK,
2 NL,NL1,NOLINE,NDLPNT,NDLRAD,IW,IH
READ(5,PARAM)
$ALPH=GAPPOT*100./ (BRKDWN*CONVER)
$CONST=(CONVER/100.)*2*RHOZRO/(PRMTVT*GAPPOT)
WRITE(6,PARAM)
HL=1./((NROWS-1)*1.)
WRITE(6,210) $ALPH,$CONST
DO 10 J=1,NCOLS
DO 10 I=1,NROWS
A(I,J)=0.5
B(I,J)=0.0
10 G(I,J)=0.0
19 CALL GSPRD($CONST,&34)
IF(NDIMEN.EQ.0) GO TO 34
WRITE(6,240)
WRITE(6,245) NROWS
WRITE(6,230) ((J,R(J)),J=1,NROWS)
34 CALL GENFIL(&70)
CALL CALC1($ALPH)
CALL OUTPUT(&70)
51 GO TO 70
210 FORMAT(' ',2X,5F20.10)
230 FORMAT(' ',T15,5('R(',I3,')=',F8.5,3X),/)
240 FORMAT('1')
245 FORMAT(' ',T49,'THE JET RADIUS AT STATIONS 1 THRU ',
1 I3,/)
70 STOP
END

```

```

SUBROUTINE GSPRD($CONST,*)
COMMON/BL3/G(81,61)
COMMON/BL5/R(81)
COMMON/BL6/NATRAD,RHOZRO,PRMTVT,GAPPOT,BRKDWN,CONVER,
1 NOZPOS,NGLOSS,NROWS,NCOLS,DELU,NBLOCK,NL,NL1,HL
COMMON/BL10/NDIMEN,NDLPNT,NDLRAD
Q=HL**2*$CONST
GLOSS=0.
IF(NDIMEN) 20,10,20
10 DO 11 I=NOZPOS,NROWS
DO 11 J=1,NCOLS
IF(NGLOSS.EQ.1) GLOSS=0.
11 G(I,J)=(1.-GLOSS)**2*Q
IF(NOZPOS-1) 20,19,20
19 RETURN 1
20 IF(NOZPOS.EQ.NDLPNT) GO TO 24
DO 21 I=1,NDLPNT
21 R(I)=(NDLRAD-1)*HL
K2=NDLPNT+1
A=((NDLRAD-1)*HL)**2
B=((NATRAD-1)*HL)**2
VARA=(A-B)/((NDLPNT-NOZPOS)*1.)
DO 23 I=K2,NOZPOS
23 R(I)=(VARA*(I-NDLPNT)+A)**.5
IF(NDIMEN.EQ.0) RETURN 1
24 A=(NROWS-NOZPOS)*1.
DO 35 I=NOZPOS,NROWS
B=(I-NOZPOS)*1.
X=B/A
35 R(I)=.0445+.0043*X+.0533*X**2
B=R(NOZPOS)
DO 50 I=NOZPOS,NROWS
DO 40 J=1,NCOLS
K1=J-1
IF(R(I)-K1*HL) 43,42,42
42 G(I,J)=(B/R(I)-GLOSS)**2*Q
GO TO 40
43 IF(R(I)-HL*(K1-.5)) 50,44,44
44 G(I,J)=(B/R(I)-GLOSS)**2*Q
GO TO 50
40 CONTINUE
50 CONTINUE
IF(NOZPOS.EQ.NDLPNT) RETURN
K1=NATRAD-1
K3=2*NATRAD
DO 90 I=K2,NOZPOS
DO 80 J=NDLRAD,K3
IF(NGLOSS.EQ.1) GLOSS=0.
NRAD=J-NDLRAD
IF(K1-J) 60,51,51
51 IF(R(I)-NRAD*HL) 53,52,52
52 G(I,J)=(B/R(I)-GLOSS)**2*Q
GO TO 60
53 IF(R(I)-HL*(NRAD-.5)) 80,54,54
54 G(I,J)=(B/R(I)-GLOSS)**2*Q
GO TO 60
60 NRAD=2*NDLRAD-J
IF(NRAD) 80,80,65
65 G(I,NRAD)=(B/R(I)-GLOSS)**2*Q
80 CONTINUE
90 CONTINUE
RETURN
END

```

```

SUBROUTINE GENFIL(*)
  COMMON/BL1/A(81,61)
  COMMON/BL2/B(81,61)
  COMMON/BL3/G(81,61)
  COMMON/BL4/NOLINE,N1,IW,IH
  COMMON/BL6/NATRAD,RHOZRO,PRMTVT,GAPPOT,BRKDWN,CONVER,
1 NOZPOS,NGLOSS,NROWS,NCOLS,DELU,NBLOCK,NL,NL1,HL
  COMMON/BL11/XLIN(4000),YLIN(4000)
  XVAL=(IW*1.)/(NCOLS*1.-1.)
  YVAL=(IH*1.)/(NROWS*1.-1.)
  N1=0
  DO 20 I=1,NBLOCK
    READ(5,200) NI1,NI2,NJ1,NJ2,PV,GV
    DO 10 I1=NI1,NI2
      DO 10 J1=NJ1,NJ2
        A(I1,J1)=PV
        B(I1,J1)=PV
        G(I1,J1)=GV
        IF(GV-98.98) 10,5,5
5      N1=N1+1
        XLIN(N1)=XVAL*(J1-1)
        YLIN(N1)=YVAL*(I1-1)
10    CONTINUE
20    CONTINUE
    IF(NOLINE) 22,21,22
21    CALL OUTPUT(&70)
70    RETURN 1
22    RETURN
200  FORMAT(4I3,2F12.3)
      END

```

```

SUBROUTINE CALC1($ALPH)
COMMON/BL1/A(81,61)
COMMON/BL2/B(81,61)
COMMON/BL3/G(81,61)
COMMON/BL5/R(81)
COMMON/BL6/NATRAD,RHOZRO,PRMTVT,GAPPOT,BRKDWN,CONVER,
1INOZPOS,NGLOSS,NROWS,NCOLS,DELU,NBLOCK,NL,NL1,HL
COMMON/BL10/NDIMEN,NDLPNT,NDLRAD
ITCNT=1
ITERS=1
5 DO 20 J=1,NCOLS
  J1=J+1
  J2=J-1
  R1=J2*HL
  IF(R1) 7,7,8
8  ARG1=.5*HL/R1
7  DO 15 I=1,NROWS
    I1=I+1
    I2=I-1
    IF(G(I,J).GT.98..AND.G(I,J).LT.100.) GO TO 15
    IF(J.EQ.1.OR.J.EQ.NCOLS) GO TO 11
    IF(I.EQ.1.OR.I.EQ.NROWS) GO TO 16
    IF(NDIMEN) 10,10,9
9    A(I,J)=B(I,J)+1.5*(.25*(G(I,J)+ARG1*(A(I,J1)-A(I,J2))
1   +A(I,J1)+A(I,J2)+A(I1,J)+A(I2,J))-B(I,J))
    GO TO 15
10   A(I,J)=B(I,J)+1.5*(.25*(G(I,J)+A(I,J1)+A(I,J2)+A(I1,J)
1   +A(I2,J))-B(I,J))
    GO TO 15
11   IF(J.EQ.NCOLS) GO TO 12
    A(I,J)=B(I,1)+1.5*(1.333*A(I,2)-.333*A(I,3)-B(I,1))
    GO TO 15
12   J3=J-2
    A(I,J)=B(I,J)+1.5*(1.333*A(I,J2)-.333*A(I,J3)-B(I,J))
    GO TO 15
16   IF(I.EQ.NROWS) GO TO 18
    A(1,J)=B(1,J)+1.5*(1.333*A(2,J)-.333*A(3,J)-B(1,J))
    GO TO 15
18   I3=I-2
    A(I,J)=B(I,J)+1.5*(1.333*A(I2,J)-.333*A(I3,J)-B(I,J))
15  CONTINUE
20  CONTINUE
    DELMAX=0.
    DO 24 J=1,NCOLS
      DO 24 I=1,NROWS
        DEL=A(I,J)-B(I,J)
        ADEL=ABS(DEL)
        IF(ADEL.GT.DELMAX) DELMAX=ADEL
24  CONTINUE
    IF(DELU-DELMAX) 26,40,40
26  DO 34 J=1,NCOLS
    DO 34 I=1,NROWS
34  B(I,J)=A(I,J)
    IF(ITCNT-100) 36,35,35
35  WRITE(6,210) ITERS,DELMAX
    ITCNT=1
    ITERS=ITERS+1
    GO TO 5
36  ITERS=ITERS+1
    ITCNT=ITCNT+1
    GO TO 5
40  WRITE(6,320) ITERS
    WRITE(6,230)
    WRITE(6,232)
    CALL WRITER(A,NROWS,NCOLS)
    ARG2=.5/HL*$ALPH
    DO 45 J=1,NCOLS
      J1=J+1

```



```

J2=J-1
J3=J+2
J4=J-2
DO 45 I=1,NROWS
  I1=I+1
  I2=I-1
  I3=I+2
  I4=I-2
  IF(I.EQ.1.OR.I.EQ.NROWS) GO TO 41
  AZ=A(I2,J)-A(I1,J)
  GO TO 42
41 IF(I.EQ.1) AZ=A(3,J)+3.*A(1,J)-4.*A(2,J)
  IF(I.EQ.NROWS) AZ=4.*A(I2,J)-A(I4,J)-3.*A(I,J)
42 IF(J.EQ.1.OR.J.EQ.NCOLS) GO TO 43
  AR=A(I,J2)-A(I,J1)
  GO TO 44
43 AR=0.0
44 B(I,J)=ARG2*AZ
  G(I,J)=ARG2*AR
45 CONTINUE
  WRITE(6,230)
  WRITE(6,237)
  CALL WRITER(B,NROWS,NCOLS)
  WRITE(6,230)
  WRITE(6,239)
  CALL WRITER(G,NROWS,NCOLS)
  EMAX=0.0
  DO 55 J=1,NCOLS
    DO 55 I=1,NROWS
      SUM=B(I,J)**2+G(I,J)**2
      B(I,J)=SQRT(SUM)
      IF(B(I,J).GT.EMAX) EMAX=B(I,J)
55 CONTINUE
  WRITE(6,230)
  WRITE(6,234)
  WRITE(6,235) EMAX
  CALL WRITER(B,NROWS,NCOLS)
  IF(NDIMEN) 58,58,109
109 DO 49 I=1,NROWS
  IF(R(I)) 110,110,120
110 DO 113 J=1,NCOLS
113 G(I,J)=1.+1.*(J-1)
  GO TO 49
120 XSLP=1./R(I)
  DO 49 J=1,NCOLS
  G(I,J)=XSLP*HL*(J-1)
  49 CONTINUE
210 FORMAT(' ',T5,'AFTER',I5,1X,'ITERATIONS--DELMAX=',
1F11.5,/)
230 FORMAT('1')
232 FORMAT(' ',T49,'THE MATRIX OF POTENTIALS',/)
234 FORMAT(' ',T51,'THE |E| FIELD MATRIX',/)
235 FORMAT(' ',T42,'MAXIMUM FIELD STRENGTH IS',F12.4,/)
237 FORMAT(' ',T46,'AXIAL COMPONENTS OF |E| FIELD',/)
239 FORMAT(' ',T47,'RADIAL COMPONENTS OF |E| FIELD',/)
320 FORMAT(' ',T37,'THE POTENTIAL ITERATION SCHEME HAS',
1T37,'CONVERGED IN',I5,' ITERATIONS',/)
58 RETURN
END

```

```

SUBROUTINE WRITER(Z,NROWS,NCOLS)
DIMENSION Z(81,61)
J1=1
J2=10
10 DO 15 I=1,NROWS
  IF(J2.GE.NCOLS) J2=NCOLS
15 WRITE(6,220) I,(Z(I,J),J=J1,J2)
  IF(J2.EQ.NCOLS) RETURN
  J1=J1+10
  J2=J2+10
  WRITE(6,230)
  GO TO 10
220 FORMAT(' ',I3,10F12.4)
230 FORMAT('1')
END

```

```

SUBROUTINE CLVL(CM,CLM,NUML)
COMMON/BL6/NATRAD,RHOZRO,PRMTVT,GAPPOT,BRKDOWN,CONVER,
1 NOZPOS,NGLOSS,NROWS,NCOLS,DELU,NBLOCK,NL,NL1,HL
DIMENSION CM(81,61),CLM(NUML)
CMIN=CM(1,1)
CMAX=CMIN
DO 5 J=1,NCOLS
DO 5 I=1,NROWS
  IF(CM(I,J).LT.CMIN) CMIN=CM(I,J)
  IF(CM(I,J).GT.CMAX) CMAX=CM(I,J)
5 CONTINUE
C NOW DETERMINE CONTOUP LEVELS TO BE PLOTTED.
  J=NUML
  I=NUML-1
  ANL=I*1.
  PLINT=(CMAX-CMIN)/ANL
C NOW FILL THE CONTOUR LEVEL VECTOR
DO 6 I=1,J
6 CLM(I)=CMIN+(I-1)*PLINT
RETURN
END

```

```

SUBROUTINE FLOP(Z,NROWS,NCOLS)
DIMENSION Z(81,61)
IIVRT=NROWS/2
DO 3 I=1,IIVRT
  M=NROWS-(I-1)
  DO 3 J=1,NCOLS
    SAVE=Z(I,J)
    Z(I,J)=Z(M,J)
3 Z(M,J)=SAVE
RETURN
END

```

```

SUBROUTINE OUTPUT(*)
REAL*8 TITLE(30)/'          ','          ','          ','          ',
1 '          ','          ','          ','          ',
2 '          ','          ','          ','          ',
3 '          ','          ','          ','          ',
4 'GAPPOT          ','          ','          ','          ',
5 '          ','          ','          ','          ',
6 '          ','          ','          ','          ',
7 'AL MAP          ','          ','          ','          ',
REAL*8 TITLEA(2)/'|E| FIEL','D MAP  '/
REAL*8 TITLEB(2)/' GEOMET','RY PLOT '/
REAL*8 TABLE(6)
LOGICAL*1 LTG(3)
COMMON/BL1/A(81,61)
COMMON/BL2/B(81,61)
COMMON/BL3/G(81,61)
COMMON/BL4/NOLINE,N1,IW,IH
COMMON/BL5/R(81)
COMMON/BL6/NATRAD,RHCZRO,PRMTVT,GAPPOT,BRKDOWN,CONVER,
1 NOZPOS,NGLOSS,NROWS,NCOLS,DELU,NBLOCK,NL,NL1,HL
COMMON/BL7/CL(30)
COMMON/BL8/CL1(30)
COMMON/BL9/CL2(1)
NAMELIST/TABL/TABLE,LTG
READ(5,TABL)
C FIRST FIGURE CONTOUR LEVELS TO BE PLOTTED FOR MATRIX A
C CALL CLVL(A,CL,NL)
C NOW FIGURE CONTOUR LEVELS FOR |E| FIELD.
C CALL CLVL(B,CL1,NL1)
C THE CONTOUR LEVEL VALUE FOR THE CLOUD BOUNDARY IS 1.0
CL2(1)=1.0
WRITE(6,210)
DO 3 I=1,NL
3 WRITE(6,215) I,CL(I),I,CL1(I)
CALL FLOP (A,NROWS,NCOLS)
CALL FLOP (B,NROWS,NCOLS)
CALL FLOP (G,NROWS,NCOLS)
TITLE(8)=TABLE(1)
TITLE(11)=TABLE(4)
TITLE(14)=TABLE(2)
TITLE(17)=TABLE(3)
TITLE(20)=TABLE(5)
TITLE(23)=TABLE(6)
IF(NOLINE) 7,6,7
6 TITLE(27)=TITLEB(1)
TITLE(28)=TITLEB(2)
7 CALL CONTUR(A,NROWS,NCOLS,81,CL,NL,TITLE,LTG,G,CL2,
11,&20)
C NOW PLOT |E| FIELD CONTOURS.
TITLE(27)=TITLEA(1)
TITLE(28)=TITLEA(2)
CALL CONTUR(B,NROWS,NCOLS,81,CL1,NL1,TITLE,LTG,G,
1CL2,1,&20)
210 FORMAT(' ',T26,'THE POTENTIAL LEVELS PLOTTED',T80,
1'THE |E| FIELD LEVELS PLOTTED',/)
215 FORMAT(' ',T33,'CL(',I2,')=',F8.4,T87,'CL1(',I2,')=',
1F8.4,/)
20 IF(NOLINE) 12,10,12
10 RETURN 1
12 RETURN
END

```

```

SUBROUTINE CONTUR(AM,M,N,MX,CL,NL,TITLE,LTG,G,CL2,NL2,
1*)
REAL*8 TITLE(1)
REAL*8 WIDTH/'WIDTH'/,HEIGHT/'HEIGHT'/,WHICH
DIMENSION AM(MX,1),CL(1)
DIMENSION G(MX,1),CL2(1)
DIMENSION REC(900), X(1800), Y(1800)
DIMENSION IPT(3,3),INX(8),INY(8)
COMMON /DAYHOF/ MT,NT,NI,IX,IY,IDX,IDY,ISS,IT,IV,NP,
1NQ,JT,PY,REC,CV,IPT,INX,INY,DL,RA,THE
COMMON /INTFAC/ X,Y
DIMENSION DITSX(5),DITSY(5)
LOGICAL*1 LTG(1),MINUS,LABL
COMMON/TABL/ TABC(20,6),JC
COMMON/DITS/XMIN,YMIN,SLOPEX,SLOPEY,DITS DX,DITS DY,
1IDIR,LABL,MINUS
COMMON/BL4/NOLINE,N1,IW,IH
COMMON/BL10/NDIMEN,NDLPNT,NDLRAD
COMMON/BL13/NSCN
JC=0
LABL=LTG(1)
C CHECK IW PARAMETER
WHICH=WIDTH
IF(IW) 1,1,2
1 WRITE(6,60) WHICH
60 FORMAT('0',T7,A8,'OF CONTOUR GRAPH ILLEGAL.')
71 WRITE(6,64)
64 FORMAT('0',T7,'NO GRAPH WILL BE PRODUCED.')
RETURN
C CHECK IF IW IS TOO WIDE
2 IF(IW-9) 3,3,40
40 WRITE(6,61)
61 FORMAT('0',T7,'IW PARAMETER GREATER THAN 9. CONTUR
1 WILL SET IW=9.')
IW=9
C NOW CHECK IH PARAMETER
3 IF(IH) 4,4,5
4 WHICH=HEIGHT
GO TO 1
5 DITS DX=(N-1.0)/IW
DITS DY=(-1.0+M)/IH
XMIN=1.0
YMIN=-M
SLOPEX=1.0/DITS DX
SLOPEY=1.0/DITS DY
DITSX(1)=1.0
DITSX(4)=1.0
DITSX(5)=1.0
DITSX(2)=N
DITSX(3)=N
DITSY(1)=-1.0
DITSY(2)=-1.0
DITSY(5)=-1.0
DITSY(3)=-M
DITSY(4)=-M
DO 2011 I=1,5
2011 DITSX(I)=SLOPEX*(DITSX(I)-XMIN)
DITSY(I)=SLOPEY*(DITSY(I)-YMIN)
STARTP=(9.0-IW)/2.0
CALL PLOTS
CALL PLOT(STARTP,0.0,-3)
CALL LINE(DITSX,DITSY,5,1,1)
DITSX(1)=DITSX(1)-.5
DITSX(5)=DITSX(1)
DITSX(4)=DITSX(4)-.5
DITSX(2)=DITSX(2)+.5
DITSX(3)=DITSX(3)+.5
DITSY(1)=DITSY(1)+.5

```

```

DITSY(5)=DITSY(1)
DITSY(2)=DITSY(2)+.5
DITSY(3)=DITSY(3)-.5
DITSY(4)=DITSY(4)-.5
CALL LINE(DITSX,DITSY,5,1,1)
SLOPEX=1.0/DITS DX
SLOPEY=1.0/DITS DY
IENDX=SLOPEX*N+1
IENDY=SLOPEY*M+1
IF(.NOT.LTG(2)) GO TO 34
C DRAW TIC MARKS ON OUTER FRAME
C START ON LEFT EDGE GOING DOWNWARD
IFLAG=0
ZINGX=-.1
ZINGY=0.0
ZX=0.0
ZY=-1.0
CX=DITSX(1)
CY=DITSY(1)-.5
IEND=IENDY
2222 IFLAG=IFLAG+1
DO 2022 I=1,IEND
CALL PLOT(CX,CY,3)
COORDX=CX+ZINGX
COORDY=CY+ZINGY
CALL PLOT(COORDX,COORDY,2)
CX=CX+ZX
2022 CY=CY+ZY
GO TO (21,22,23,24),IFLAG
C NOW DO THE RIGHT EDGE GOING DOWNWARD
21 ZINGX=.1
CX=DITSX(2)
CY=DITSY(2)-.5
GO TO 2222
C NOW DO TOP EDGE
22 ZINGX=0.0
ZINGY=.1
ZX=1.0
ZY=0.0
CX=DITSX(1)+.5
CY=DITSY(1)
IEND=IENDX
GO TO 2222
C NOW DO THE BOTTOM EDGE
23 ZINGY=-.1
CX=DITSX(4)+.5
CY=DITSY(4)
ZINGY=-.1
GO TO 2222
C NOW LABEL TIC MARKS
C DO X-DIRECTION FIRST, TOP EDGE
C POSITION PEN
24 DELTAX=DITS DX
IFLAG=0
ZX=1.0
ZY=0.0
CX=DITSX(1)+.35
CY=DITSY(1)+.12
3033 IFLAG=IFLAG+1
XZERO=1.0
DO 3333 I=1,IEND
CALL NUMBER(CX,CY,.14,XZERO,0.0,1)
CX=CX+ZX
CY=CY+ZY
3333 XZERO=XZERO+DELTAX
GO TO (31,32,33,34),IFLAG
C LABEL BOTTOM EDGE TIC MARKS
31 CX=DITSX(4)+.35
CY=DITSY(4)-.19
GO TO 3033
C LABEL LEFT EDGE OF TIC MARKS
32 CX=DITSX(4)-.4

```



```

        CY=DITSY(4)+.46
        DELTAX=DITSY(4)
        IEND=IENDY
        ZX=0.0
        ZY=1.0
        GO TO 3033
C      NOW LABEL RIGHT EDGE TIC MARKS
33     CX=DITSX(3)+.12
        CY=DITSY(3)+.46
        GO TO 3033
C      CHECK IF GRID DESIRED
34     CALL RESTOF(LTG,IENDX,IENDY,NL,AM,M,N,MX,CL,NL2,G,CL2,
1      STARTP,TITLE,DITSX,DITSY)
        IF(NOLINE) 2502,2505,2502
2502    RETURN
2505    RETURN 1
        END

```

```

SUBROUTINE RESTOF(LTG,IENDX,IENDY,NL,AM,M,N,MX,CL,NL2,
2,TITLE,DITSX,DITSY)
REAL*8 TITLE(1)
DIMENSION AM(MX,1),CL(1)
DIMENSION G(MX,1),CL2(1)
DIMENSION DITSX(5),DITSY(5)
LOGICAL*1 LTG(1),MINUS,LABL
COMMON/TABL/TABC(20,6),JC
COMMON/DITS/XMIN,YMIN,SLOPEX,SLOPEY,DITSX,DITSY,
1IDIR,LABL,MINUS
COMMON/BL4/NOLINE,N1,IW,IH
COMMON/BL10/NDIMEN,NDLPNT,NDLRAD
COMMON/BL11/XLIN(4000),YLIN(4000)
COMMON/BL13/NSCN
IF(.NOT.LTG(3)) GO TO 35
C      DRAW INCH BY INCH GRID
C      IEND=IENDX-2
C      POSITION PEN
        IFLAG=0
        CX=DITSX(1)+.5
        CY=DITSY(1)-.5
        COORDX=0.0
        COORDY=-IH
        DX=1.0
        DY=0.0
4044    DO 4444 I=1,IEND
        CX=CX+DX
        CY=CY+DY
        CALL PLOT(CX,CY,3)
        ZX=CX+COORDX
        ZY=CY+COORDY
4444    CALL PLOT(ZX,ZY,2)
        IF(IFLAG) 35,42,35

```

```

42  IFLAG=1
    IEND=IENDY-2
    CY=DITSY(4)+.5
    CX=DITSX(4)+.5
    COORDX=IW
    COORDY=0.0
    DX=0.0
    DY=1.0
    GO TO 4044
35  CONTINUE
    IF(NOLINE) 11,2500,2500
2500 CALL LINE(XLIN,YLIN,N1,1,-6)
    IF(NOLINE) 11,779,11
    11 DO 20 I=1,NL
    20 CALL SCAN(AM,M,N,MX,CL(I))
    NSCN=1
    IF(NDIMEN) 2002,2003,2002
    2002 DO 2004 I=1,NL2
    2004 CALL SCAN(G,M,N,MX,CL2(I))
    2003 IF(.NOT.LABL) GO TO 778
    IF(JC.EQ.0) GO TO 778
    DO 777 I=1,JC
    COORDX=TABC(I,4)
    COORDY=TABC(I,5)
    CLEV=TABC(I,6)
    CALL NUMBER(COORDX,COORDY,.07,CLEV,0.0,3)
777  CONTINUE
778  CALL SYMBOL(-STARTP,IH+1.0,.21,TITLE(25),0.0,48)
    CALL SYMBOL(-STARTP,IH+1.5,.21,TITLE(19),0.0,48)
    CALL SYMBOL(-STARTP,IH+2.0,.21,TITLE(13),0.0,48)
    CALL SYMBOL(-STARTP,IH+2.5,.21,TITLE(7),0.0,48)
    CALL SYMBOL(-STARTP,IH+3.0,.21,TITLE(1),0.0,48)
    CALL PLOT(-STARTP,IH+6.5,-3)
    CALL PLOTE
    RETURN
779  CALL SYMBOL(-STARTP,IH+1.0,.21,TITLE(25),0.0,48)
    CALL PLOT(-STARTP,IH+4.5,-3)
    CALL PLOTE
    RETURN
END

```

```

SUBROUTINE SCAN(AM,M,N,MX,CL)
DIMENSION AM(MX,1),REC(900), X(1800), Y(1800)
DIMENSION IPT(3,3),INX(8),INY(8)
COMMON /DAYHOF/ MT,NT,NI,IX,IY,IDX,IDY,ISS,IT,IV,NP,NQ
1 COMMON /INTFAC/ X,Y
LOGICAL *1 LABL,MINUS
COMMON/DITS/XMIN,YMIN,SLOPEX,SLOPEY,DITS DX,DITS DY,
1 IDIR,LABL,MINUS
COMMON/BL13/NSCN
D=0.
R=1.
TH = 1.570796
NP=0
DL=D
RA=R
THE=TH
MT=N
NT=M
CV=CL
IF(NSCN.EQ.1) IZW=0
IF(IZW-120631) 1,3,1
1 IPT(1,1)=8
IPT(1,2)=1
IPT(1,3)=2
IPT(2,1)=7
IPT(2,3)=3
IPT(3,1)=6
IPT(3,2)=5
IPT(3,3)=4
INX(1)=-1
INX(2)=-1
INX(3)=0
INX(4)=1
INX(5)=1
INX(6)=1
INX(7)=0
INX(8)=-1
INY(1)=0
INY(2)=1
INY(3)=+1
INY(4)=+1
INY(5)=0
INY(6)=-1
INY(7)=-1
INY(8)=-1
IZW=120631
3 XT=MT
DO 58 J=1,900
58 REC(J)=0
ISS=0
2 MT1=MT-1
IDIR=1
DO 110 I=1,MT1
IF(AM(1,I)-CV) 55,110,110
55 IF(AM(1,I+1)-CV) 110,57,57
57 IX=I+1
IY=1
IDX=-1
IDY=0
CALL TRACE (AM,MX)
110 CONTINUE
NT1=NT-1
IDIR=2
DO 20 I=1,NT1
IF(AM(I,MT)-CV) 15,20,20
15 IF(AM(I+1,MT)-CV) 20,17,17
17 IX=MT
IY=I+1
IDX=0

```

```

IDY=-1
CALL TRACE (AM,MX)
20 CONTINUE
IDIP=3
22 DO 30 I=1,MT1
MT2=MT+1-I
IF(AM(NT,MT2)-CV) 25,30,30
25 IF(AM(NT,MT2-1)-CV) 30,27,27
27 IX=MT2-1
IY=NT
IDX=1
IDY=0
CALL TRACE (AM,MX)
30 CONTINUE
IDIR=4
DO 40 I=1,NT1
NT2=NT+1-I
IF(AM(NT2,1)-CV) 35,40,40
35 IF(AM(NT2-1,1)-CV) 40,37,37
37 IX=1
IY=NT2-1
IDX=0
IDY=1
CALL TRACE (AM,MX)
40 CONTINUE
IDIR=5
ISS=1
NT1=NT-1
MT1=MT-1
DO 10 J=2,NT1
DO 10 I=1,MT1
IF(AM(J,I)-CV) 5,10,10
5 IF(AM(J,I+1)-CV) 10,7,7
7 COM=100*(I+1)+J
IF (NP) 12,11,12
12 DO 9 ID= 1,NP
IF (REC(ID)-COM) 9,10,9
9 CONTINUE
11 IX= I+1
IY=J
IDX=-1
IDY=0
CALL TRACE (AM,MX)
10 CONTINUE
RETURN
END

```

```

SUBROUTINE TRACE (AM,MY)
DIMENSION AM(MY,1),REC(900), X(1800), Y(1800)
DIMENSION IPT(3,3), INX(8), INY(8)
COMMON /DAYHOF/ MT,NT,NI,IX,IY,IDX,IDY,ISS,IT,IV,NP,
1N ,JT,PY,REC,CV,IPT,INX,INY,DL,RA,THE
COMMON /INTFAC/ X,Y
PY=0.0
RC= COS (THE)*RA
RS= SIN (THE)*RA
501 JT=0
N=0
IX0=IX
IY0=IY
ISX=IDX+2
ISY=IDY+2
IS=IPT(ISX,ISY)
JTB=0
ISO=IS
IF(ISO-8) 18,18,17
17 ISO=ISO-8
18 IT=0
5 CONTINUE
CALL CALC (AM,MY)
NZ=N
N=NZ
IF (IT+JT-1) 49,49,47
47 XS=X(N-1)
YS=Y(N-1)
X(N-1)=X(N)
Y(N-1)=Y(N)
X(N)=XS
Y(N)=YS
49 IS=IS+1
JT=IT
9 IF (IS-9) 8,7,7
7 IS=IS-8
8 IDX=INX(IS)
IDY=INY(IS)
IX2=IX+IDX
IY2=IY+IDY
JTB=JTB+1
IF (JTB-1799) 51,51,308
308 PRINT 103,CV,X(N),Y(N)
103 FORMAT(1H0,23HA CONTCUR LINE AT LEVEL,E12.5,
121H WAS TERMINATED AT X=,E12.5,3H Y=,E12.5/
2 48H BECAUSE IT CONTAINED MORE THAN 1799 PLOT POINTS
RETURN
51 CONTINUE
IF (ISS) 10,10,20
20 IF(IX-IX0) 12,21,12
21 IF(IY-IY0) 12,22,12
22 IF(IS-ISO) 12,23,12
23 CONTINUE
CALL CALC (AM,MY)
GO TO 73
10 IF(IX2) 13,50,13
13 IF (IX2-MT) 19,19,50
19 IF (IY2) 11,50,11
11 IF (IY2-NT) 12,12,50
12 IF(CV-AM(IY2,IX2)) 206,206,5
206 IF (IDX**2+IDY**2-1) 213,6,213
213 DCP=(AM(IY,IX)+AM(IY,IX2)+AM(IY2,IX)+AM(IY2,IX2))/4.0
IF (DCP-CV) 5,217,217
217 IF (INX(IS-1)) 214,215,214
214 IX=IX+IDX
IDX=-IDX
PY=2.0
CALL CALC (AM,MY)

```



```

IX=IX+IDX
GO TO 6
215 IY=IY+IDY
IDY=-IDY
PY=2.0
CALL CALC (AM,MY)
IY=IY+IDY
6 IF(AM(IY,IX-1)-CV) 306,16,16
306 NP=NP+1
REC(NP)=100*IX+IY
16 IS=IS+5
IX=IX2
IY=IY2
GO TO 9
50 XT=MT
IF(AM(IY,IX-1)-CV) 307,73,73
307 NP=NP+1
REC(NP)=100*IX+IY
73 DO 74 I=1,N
74 X(I)=X(I)+RC*Y(I)
Y(I)=RS*Y(I)
CALL PLOTT(N,CV)
RETURN
END

```

```

SUBROUTINE CALC(AM,MY)
DIMENSION AM(MY,1),REC(900), X(1800), Y(1800)
DIMENSION IPT(3,3),INX(8),INY(8)
COMMON /DAYHOF/ MT,NT,NI,IX,IY,IDX,IDY,ISS,IT,IV,NP,N,
1 JT,PY,REC,CV,IPT,INX,INY,DL,RA,THE
COMMON /INTFAC/ X,Y
IT=0
N=N+1
IF (IDX**2 + IDY**2 -1) 20,1,20
1 IF (ICX) 10,2,10
2 X(N)=IX
Z=IY
IY2=IY+IDY
DY=IDY
41 Y(N)=((AM(IY,IX)-CV)/(AM(IY,IX)-AM(IY2,IX)))*DY+Z
RETURN
10 Y(N)=IY
W=IX
DX=IDX
IX2=IX+IDX
44 X(N)=((AM(IY,IX)-CV)/(AM(IY,IX)-AM(IY,IX2)))*DX+W
RETURN
20 IX2=IX+IDX
IY2=IY+IDY
W=IX
Z=IY
DX=IDX
DY=IDY
DCP=(AM(IY,IX)+AM(IY,IX2)+AM(IY2,IX)+AM(IY2,IX2))/4.0
IF (PY-2.0) 24,21,24
24 IF (DCP-CV) 21,21,25
21 AL=AM(IY,IX)-DCP
23 V=.5*(AL+DCP -CV)/AL
27 X(N)=V*DX+W
Y(N)=V*DY+Z
PY=0.0
RETURN
25 IT=1
AL=AM(IY2,IX2)-DCP
33 V=.5*(AL+DCP-CV)/AL
28 X(N)=-V*DX+W + DX
Y(N)=-V*DY+Z + DY
Y(N)=-V*DY+Z + DY
RETURN
END

```

```

SUBROUTINE PLOTT(NP,CV)
COMMON/INTFAC/X(1800),Y(1800)
LOGICAL*1 MINUS,LABL
COMMON/TABL/ TABC(20,6),JC
COMMON/DITS/XMIN,YMIN,SLOPEX,SLOPEY,DITS DX,DITS DY,
C 1 IDIR,LABL,MINUS
SCALE POINTS FOR PLOT ROUTINE
DO 100 I=1,NP
X(I)=SLOPEX*(X(I)-XMIN)
100 Y(I)=SLOPEY*(-Y(I)-YMIN)
CALL LINE(X,Y,NP,1,1)
IF(.NOT.LABL) RETURN
DIR=0.0
GO TO (1,2,3,4,6), IDIR
1 DIR=90.
2 COORDX=X(1 )
COORDY=Y(1 )
5 CALL NUMBER(COORDX,COORDY,.07,CV,DIR,3)
RETURN
C MOVE PEN DOWN ONE HALF INCH
3 DIR=90.
COORDX=X(1 )
COORDY=Y(1 )-.3
GO TO 5
C MOVE PEN TO THE LEFT
4 COORDX=X(1 )-.3
COORDY=Y(1 )
GO TO 5
C SEARCH FOR XMAX,XMIN,YMAX,YMIN,AND SAVE YMINX
6 XMAX=X(1)
SMIN=XMAX
YMINX=Y(1)
YMAX=YMINX
VMIN=YMINX
DO 200 I=2,NP
IF(X(I).GT.XMAX) XMAX=X(I)
IF(Y(I).LT.VMIN) VMIN=Y(I)
IF(Y(I).GT.YMAX) YMAX=Y(I)
IF(X(I).GE.SMIN) GO TO 200
SMIN=X(I)
YMINX=Y(I)
200 CONTINUE
C JC=NUMBER OF ENTRIES IN TABC
IF(JC) 400,500,400
400 DO 900 I=1,JC
IF(XMAX.LT.TABC(I,1).AND.YMAX.LT.TABC(I,2).AND.VMIN.
1GT.TABC(I,3).AND.SMIN.GT.TABC(I,4)) GO TO 700
900 CONTINUE
C DID NOT FIND THIS CONTOUR TO BE INTERIOR TO ANOTHER
C CHECK IF EXTERIOR
DO 1000 I=1,JC
IF(XMAX.GT.TABC(I,1).AND.YMAX.GT.TABC(I,2).AND.VMIN.
1LT.TABC(I,3).AND.SMIN.LT.TABC(I,4)) GO TO 800
1000 CONTINUE
500 IF (JC.EQ.20) RETURN
JC=JC+1
MC=JC
600 TABC(MC,1)=XMAX
TABC(MC,2)=YMAX
TABC(MC,3)=VMIN
TABC(MC,4)=SMIN
TABC(MC,5)=YMINX
TABC(MC,6)=CV
RETURN
C CHECK IF THIS INTERIOR ONE IS OF HIGHER LEVEL
700 IF(CV.LE.TABC(I,6) ) RETURN

```

```
2000 MC=I
      GO TO 600
C     CHECK IF LEVEL OF THIS EXTERIOR ONE IS HIGHER
      800 IF(CV.LT.TABC(I,6)) RETURN
      GO TO 2000
      END
```





## APPENDIX

### BIBLIOGRAPHY

1. Moore, A.D., "Electrostatics," Scientific American, Vol. 226, pp. 47-58, March 1972.
2. Aerospace Research Laboratories (ARL 68-0156), Computer Program for the Calculation of Electric Fields in an Electrofluidynamic Generator, by John E. Minardi, p. 1, August 1968.
3. Alston, L.L. and others, High-Voltage Technology, p. 17, Oxford University Press, 1968.
4. United States Naval Postgraduate School Report NPS-57Z10121A, EHD Research Final Report for the Year 1969-70, by Oscar Biblarz, K.E. Woehler, and T.H. Gawain, p. 9, 30 December 1970.
5. United States Naval Postgraduate School Report NPS-57ZI912A, EHD Research Final Report for the Year 1968-69, by Oscar Biblarz, p. 2, 30 December 1960.
6. Biblarz, O., "Analysis of Optimum Charged Particle Size Based on the Conversion Efficiency of Electrogasdynamic Generators," Energy Conversion, v. 10, p. 207-212, 1970.
7. Laib, R.J., Spectral Anemometry with an Electrogasdynamic Probe, M.S. Thesis, United States Naval Postgraduate School, 1971.
8. AGARDograph 122, Some Analytical Treatments of EFD Processes, by J.E. Minardi, pp. 125-179, December 1968.
9. Ryder, J.D., Electronic Fundamentals and Applications, p. 104, Prentice-Hall, Inc., 1960.
10. Todd, J., and others, Survey of Numerical Analysis, p. 393, McGraw-Hill, 1962.
11. Cobine, J.D., Gaseous Conductors, pp. 173-178, McGraw-Hill, 1941.
12. Shapiro, A.H., The Dynamics and Thermodynamics of Compressible Fluid Flow, Vol. 1, The Ronald Press Company, 1953.
13. Blatt, J.M., Introduction to FORTRAN IV Programming: Using the WATFOR Compiler, Goodyear Publishing Company, 1968.
14. Darrow, K.K., Electrical Phenomena in Gases, pp. 209-212, The Williams & Wilkins Company, 1932.



# DISTRIBUTION LIST

	No. Copies
1. Defense Documentation Center Cameron Station Alexandria, Virginia 22314	20
2. Library Naval Postgraduate School Monterey, California 93940	2
3. Commander Naval Air Systems Command Department of the Navy Attn: Dr. H. R. Rosenwasser, Code AIR-310C	1
4. Chairman Department of Aeronautics Naval Postgraduate School Monterey, California 93940	1
5. Professor Oscar Biblarz Department of Aeronautics Naval Postgraduate School Monterey, California 93940	5
6. Professor J. R. Melcher Dept. of Elec. Engr., Room 31-141 Mass. Inst. of Technology Cambridge, Massachusetts 02139	1
7. Professor Albert Solbes Dept. of Aero., Room 37-375 Mass. Inst. of Technology Cambridge, Massachusetts 02139	1
8. Mr. Alvin M. Marks Marks Polarized Corp. 153-16 10th Avenue Whitestone, New York 11357	1
9. Dr. M. C. Gourdine Gourdine Systems, Inc. 112 Naylon Avenue Liningston, New Jersey 07039	1

10. Dr. Hans von Ohain 1  
Aerospace Research Laboratory  
U. S. Air Force  
Wright-Patterson AFB, Ohio 45433
11. Professor A. E. Fuhs 1  
Department of Aeronautics  
Naval Postgraduate School  
Monterey, California 93940
12. Dr. Ernesto Barreto 1  
Atmospheric Research Center  
State University of New York  
130 Saratoga Road  
Scotia, New York 12302
13. Professor H. R. Velkoff 1  
Dept. of Mech. Engr.  
Ohio State University  
Columbus, Ohio 43210
14. Dr. Otmar M. Stuetzer 1  
Sandia Corporation  
P. O. Box 5800  
Albuquerque, New Mexico 87115
15. Dr. Ralph Roberts 1  
Office of Naval Research  
Power Program, Code 473  
Washington, D. C. 20360
16. Mr. John A. Stakowski 1  
Office of Naval Research  
Power Program, Code 473  
Washington, D. C. 20360
17. Dr. H. J. Mueller 1  
Naval Air Systems Command  
Code AIR 310  
Washintgon, D. C.
18. Dr. S. J. Magram 1  
Army Research Office  
Arlington, Virginia 22200
19. Air Force Office of Scientific Research 1  
Washington, D. C. 20333  
Attn: Power Systems Group

20. Mr. Robert C. Hamilton 1  
Institute of Defense Analysis  
400 Army - Navy Drive  
Arlington, Virginia 22202
21. Dr. George C. Szego 1  
Institute of Defense Analysis  
400 Army - Navy Drive  
Arlington, Virginia 22202
22. Mr. S. Cohen 1  
NASA Lewis Research Center  
21000 Brookpark Road  
Cleveland, Ohio 44135
23. Mr. M. Lawson 1  
Aerospace Research Laboratory  
U. S. Air Force  
Wright-Patterson AFB, Ohio 45433
24. Dean of Research Administration 2  
Naval Postgraduate School  
Monterey, California 93940
25. Professor C. D. Hendricks 1  
Department of Electrical Engineering  
University of Illinois  
Urbana, Illinois 61801
26. CAPT Amer Chand 1  
Aerospace Research Laboratory  
U.S. Air Force  
Wright-Patterson AFB, Ohio 45433





## DOCUMENT CONTROL DATA - R &amp; D

(Security classification of title, body of abstract and indexing annotation must be entered when the overall report is classified)

1. ORIGINATING ACTIVITY (Corporate author) Naval Postgraduate School Monterey, California 93940		2a. REPORT SECURITY CLASSIFICATION Unclassified	
		2b. GROUP	
3. REPORT TITLE EHD Research Final Report for the Year 1971-72			
4. DESCRIPTIVE NOTES (Type of report and, inclusive dates)			
5. AUTHOR(S) (First name, middle initial, last name) Oscar Biblarz			
6. REPORT DATE February 1973		7a. TOTAL NO. OF PAGES	7b. NO. OF REFS 12
8a. CONTRACT OR GRANT NO. AIR TASK A310310C		9a. ORIGINATOR'S REPORT NUMBER(S) NPS-57ZI73021A	
b. PROJECT NO.			
c.		9b. OTHER REPORT NO(S) (Any other numbers that may be assigned this report)	
d.			
10. DISTRIBUTION STATEMENT This document has been approved for public release and sale; its distribution is unlimited.			
11. SUPPLEMENTARY NOTES		12. SPONSORING MILITARY ACTIVITY Naval Air Systems Command Washington, D. C. 20360	
13. ABSTRACT This report contains further considerations of the slip parameter for unsteady flow. Several important gas/particle combinations are represented and conclusions regarding electrical efficiency are given. Also, a computer study which solves the combines Laplace/Poisson equations for geometries representing the EHD channel is included. This program is used to predict the effect of voltage scheduling electrodes, and the predictions are checked out experimentally.			

### KEY WORDS

LINK A

LINK B

LINK C

ROLE

W T

ROLE

WT

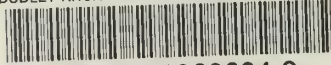
ROLE

WT

## Computer Modeling



DUDLEY KNOX LIBRARY - RESEARCH REPORTS



5 6853 01060604 9